SANDIA REPORT
SAND2024-15864
Printed November 2024

Sandia National Laboratories

Reduced-Order Modeling of Hydrogen Releases from Vent Stacks and with Wind

Melissa S. Louie, Michael C. Devin, Ethan S. Hecht, and Brian D. Ehrhart

Prepared by
Sandia National Laboratories
Albuquerque, New Mexico
87185 and Livermore,
California 94550

Issued by Sandia National Laboratories, operated for the United States Department of Energy by National Technology & Engineering Solutions of Sandia, LLC.

NOTICE: This report was prepared as an account of work sponsored by an agency of the United States Government. Neither the United States Government, nor any agency thereof, nor any of their employees, nor any of their contractors, subcontractors, or their employees, make any warranty, express or implied, or assume any legal liability or responsibility for the accuracy, completeness, or usefulness of any information, apparatus, product, or process disclosed, or represent that its use would not infringe privately owned rights. Reference herein to any specific commercial product, process, or service by trade name, trademark, manufacturer, or otherwise, does not necessarily constitute or imply its endorsement, recommendation, or favoring by the United States Government, any agency thereof, or any of their contractors or subcontractors. The views and opinions expressed herein do not necessarily state or reflect those of the United States Government, any agency thereof, or any of their contractors.

Printed in the United States of America. This report has been reproduced directly from the best available copy.

Available to DOE and DOE contractors from
U.S. Department of Energy
Office of Scientific and Technical Information
P.O. Box 62
Oak Ridge, TN 37831

Telephone: (865) 576-8401
Facsimile: (865) 576-5728
E-Mail: reports@osti.gov
Online ordering: http://www.osti.gov/scitech

Available to the public from
U.S. Department of Commerce
National Technical Information Service
5301 Shawnee Rd
Alexandria, VA 22312

Telephone: (800) 553-6847
Facsimile: (703) 605-6900
E-Mail: orders@ntis.gov
Online order: https://classic.ntis.gov/help/order-methods/



ABSTRACT

This report describes computational modeling in the HyRAM+ software for study of hydrogen behavior in two common scenarios. First, models of unignited plumes exiting a vent stack were considered. It was shown that entrainment and vent backpressure were major factors in plume physics. Second, HyRAM+ was extended to include wind effects on plumes by modifying the plume momentum balance and entrainment modeling. Use of the model showed that plume shape and length changed with wind speed and direction; in all cases, wind causes a shortening of the plume along the streamline. While the no-wind case in HyRAM+ has been validated and the newly developed wind model was fitted to very limited experimental data, more controlled experimental configurations would help validate the models and ensure accurate simulation of hydrogen plume behavior for vent stack releases or in wind.

ACKNOWLEDGEMENTS

This work was supported by the Wabtec Corporation under the direction of Chris Homison. This work was performed as part of a cooperative research and development agreement (CRADA) with the Wabtec Corporation. The authors would also like to thank Myra Blaylock, Kristin Hertz, and Chris LaFleur from Sandia National Laboratories and Chris Homison and Manoj Bhalerao from the Wabtec Corporation for their review of this document.

CONTENTS

Abstract 3
Acknowledgements 4
Executive Summary 9
Acronyms and Terms 11
1. Introduction 13
2. Modeling of a Hydrogen Release Through a Vent Stack 15
   2.1. Vent Stack Methods 15
   2.2. Vent Stack Findings 16
   2.3. Vent Stack Model Validation 28
3. Modeling of a Jet Plume in Wind 33
   3.1. Wind Modeling Methods 33
   3.2. Wind Modeling Literature Search 34
   3.3. Wind Modeling Results 37
4. Other Entrainment Models 47
5. Conclusions 53
References 55
Distribution 57

LIST OF FIGURES

Figure 2-1. Schematic showing simple vent stack model used for the study. 15
Figure 2-2. Flow chart showing workflow for vent stack calculations. 16
Figure 2-3. Vent pressure required for 750 g/s effluent flow rate for each tested vent diameter. 16
Figure 2-4. Jet plume contours showing 4 mol% concentration of hydrogen for different vent stack diameters for a constant mass flow rate of 750 g/s. 17
Figure 2-5. a) Centerline mole fraction and b) centerline velocity along the streamline of the plume for different vent stack diameters. 18
Figure 2-6. Velocity of vent stack effluent as a function of vent diameter for a constant mass flow rate of 750 g/s. 18
Figure 2-7. a) Momentum-driven entrainment calculated at the expanded orifice and b) buoyancy-driven entrainment calculated along the plume for each vent stack diameter for a constant mass flow rate of 750 g/s 20
Figure 2-8. Buoyancy-driven entrainment constant $\boldsymbol{a}$ for different vent diameters for a constant mass flow rate of 750 g/s 21
Figure 2-9. Overall entrainment calculated along the plume for each vent diameter. 23
Figure 2-10. Plumes for different vent stack diameters for a) saturated vapor, b) saturated liquid, and c) subcooled liquid storage conditions. 25
Figure 2-11. 4 mol% hydrogen concentration contours showing the comparison between plumes exiting the vent stack from compressed gaseous hydrogen and a) saturated vapor hydrogen, b) saturated liquid hydrogen, and c) subcooled liquid hydrogen from the tank. All figures show plumes for a 6 mm PRD and a 25 mm vent stack 26
Figure 2-12. Calculated vent backpressures needed at each vent temperature and for each stored phase for the mass flow rate out of the vent to match the mass flow rate out of the PRD and into the vent. 27

Figure 2-13. a) Simulation-calculated centerline mole concentrations for vertical hydrogen jets (lines) compared to slow leak experimental data (points) and b) simulated plumes out of a 1.905 mm diameter orifice. Figures taken from [3].....28
Figure 2-14. Densimetric Froude number and distance to 4% hydrogen concentration for a range of vent diameters for a constant mass flow rate of 750 g/s.....29
Figure 2-15. Simulation-calculated centerline mole concentrations for horizontal jets (lines) compared to experimental data (points). Figures taken from [5].....30
Figure 3-1. Comparison of HyRAM+ data to Grune et al. [15] data using entrainment coefficients of 0.149 for c∥ and 0.00864 for c⊥.....37
Figure 3-2. 4 mol% hydrogen concentration contours using HyRAM+ wind entrainment model, for hydrogen stored at 0.3 MPa (43 psi) and 25°C (77°F), released vertically through a 1 mm orifice, and subject to a) no wind, b) 10 m/s wind at a 0° angle, c) 10 m/s wind at a 90° angle, d) 10 m/s wind at a 270° angle, e) 10 m/s wind at a 45° angle, and f) 10 m/s wind at a 180° angle.....38
Figure 3-3. 4 mol% hydrogen concentration contours using HyRAM+ wind entrainment model, for hydrogen stored at 0.3 MPa (43 psi) and 25°C (77°F), released horizontally through a 1 mm orifice, and subject to a) no wind, b) 10 m/s wind at a 0° angle, c) 10 m/s wind at a 90° angle, d) 10 m/s wind at a 270° angle, e) 10 m/s wind at a 45° angle, and f) 10 m/s wind at a 180° angle.....40
Figure 3-4. HyRAM+ wind entrainment model behavior for 5 m/s vertically counter-flowing wind for a vertical release, showing a) contributions of different entrainment sources, b) overlay of the entrainment and the plume half-width.....41
Figure 3-5. HyRAM+ wind entrainment model behavior for 10 m/s horizontally counter-flowing wind for a horizontal release, showing a) contributions of different entrainment sources, b) overlay of the entrainment and the plume half-width.....42
Figure 3-6. 4 mol% hydrogen concentration contours using HyRAM+ wind entrainment model, for hydrogen stored at 0.3 MPa (43 psi) and 25°C (77°F), released vertically through a 1 mm orifice, and subject to a) no wind, b) 10 m/s wind at a 0° angle, c) 20 m/s wind at a 0° angle, d) 30 m/s wind at a 0° angle, e) 40 m/s wind at a 0° angle, and f) 100 m/s wind at a 0° angle. Wind vectors shown are not to scale.....43
Figure 3-7. 4 mol% hydrogen concentration contours using HyRAM+ wind entrainment model, for hydrogen stored at 0.3 MPa (43 psi) and 25°C (77°F), released horizontally through a 1 mm orifice, and subject to a) no wind, b) 10 m/s wind at a 0° angle, c) 20 m/s wind at a 0° angle, d) 30 m/s wind at a 0° angle, e) 40 m/s wind at a 0° angle, and f) 100 m/s wind at a 0° angle. Wind vectors shown are not to scale.....44
Figure 3-8. Plume streamline distance to 4 mol% hydrogen concentration for crossflow and co-flow conditions.....45
Figure 3-9. a) Downwind horizontal plume center distance and b) vertical plume center distance to the lower flammability limit for petroleum gases, provided in API RP 521, compared to hydrogen, calculated using HyRAM+.....46
Figure 4-1. Entrainment model comparison, vertical release with varying wind directions (indicated by white arrow).....49
Figure 4-2. Entrainment model comparison, horizontal release with varying wind directions (indicated by white arrow).....50
Figure 4-3. Entrainment model comparison, vertical release with counter-flowing wind of various speeds.....51

Figure 4-4. Comparison of entrainment models in Gebhart et al. [7] to experimental data from Grune et al. [15] 52

LIST OF TABLES

Table 2-1. Summary of entrainment calculations in HyRAM+ v5.1 [1]. 19
Table 2-2. Momentum and buoyancy entrainment observations for each tested vent diameter. 22
Table 2-3. Storage conditions for each phase. 23
Table 2-4. Calculated vent pressures in kPa | psi for each vent diameter and storage phase. 24
Table 2-5. Tabulated vent backpressures for each phase and vent temperature. 27
Table 3-1. Summary of 2D momentum equations adjusted to account for wind. 33
Table 3-2. Conditions for data used from Grune et al. [15]. The ambient conditions were 20°C (68°F) and 101 kPa (14.7 psi) for all cases. 36
Table 4-1. Summary of entrainment models for flowing ambient conditions from Gebhart et al. [7] 47

This page left blank

EXECUTIVE SUMMARY

Hydrogen can be an alternative fuel for locomotives, but its nascence means that its behavior in locomotive environments must be studied to ensure it is implemented safely. The two phenomena studied in this report were the release of an unignited hydrogen jet plume out of a vent stack and the behavior of hydrogen in the presence of wind that is characteristic of either naturally occurring wind or the relative wind created by movement of the locomotive. Some studies have been published on each topic, but the literature is generally high level and insufficient for building a quantitative model.

For vent stack behavior, the published studies tend to be largely qualitative and focus on the behavior of the hydrogen once it exits the vent stack, while lacking insight into the mechanisms of the flow of hydrogen through the vent stack itself. For the behavior of plumes in wind, some published work on liquid pooling experiments qualitatively shows how hydrogen plumes behave in the wind, but the scenario of interest in this study was the release of hydrogen through an orifice, which is momentum and pressure-driven in addition to buoyancy-driven. Additionally, many of the experiments were conducted outdoors so the wind speed and direction varied over time and space, it is difficult to ascertain whether a steady state was reached.

In this vent stack study, plumes were modeled in HyRAM+ based on the assumption that mass flow rate of hydrogen into the vent stack (from the pressure relief device) was the same as the flow out of the vent stack (into the ambient air), but the diameter was different at these two points. It was observed that unchoked flows tended to have a generally wider shape while choked flows were narrower. Additionally, increasing the vent diameter, which was associated with a decreased effluent velocity and Froude number, led to more of the entrainment of the plume being dominated by buoyancy rather than momentum. Unintuitively, the plume length was observed to increase with increasing vent diameter, potentially because less momentum-driven entrainment corresponds to less turbulent mixing and dilution of hydrogen in air. More hydrogen plume experiments involving vent stacks would be needed to see if the model is accurately predicting behavior or if there is an error or other unaccounted-for phenomenon missing from the model.

In the wind modeling study, wind effects were added to the existing HyRAM+ models, affecting both the momentum balance and the entrainment. Model results with entrainment constants proportional to the relative parallel and orthogonal wind velocity in a generic model were compared to data from a published experiment involving hydrogen plumes in an enclosed chamber under varying wind speeds and directions. Visualizations showed intuitive trends except for the counter-flow condition, where a horizontal plume extended rather than decreased in size, indicating a need for additional model modification. This wind entrainment model was compared to historical entrainment models plumes flowing in varied ambient conditions, revealing similar contours in response to the wind but increased overall entrainment by the historical models, contrary to the experimental data. As with the vent stack study, more data could help develop an improved model, and observing plumes with parametric variations like orifice diameter and backpressure could help define the boundary conditions for which the model is valid.

In this report, computational modeling of vent stack releases and releases into wind are presented, as they are two common scenarios that could happen on a hydrogen locomotive under normal operation. Aspects of each model were validated either quantitatively or only qualitatively in some cases using existing literature. However, more data from focused experiments simulating locomotive applications specifically could help refine the models and make them more usable for understanding the safety implications of hydrogen on locomotives.

This page left blank

ACRONYMS AND TERMS

Acronym/Term	Definition
API	American Petroleum Institute
HyRAM+	Hydrogen Plus Alternative Fuels Risk Assessment Models
PRD	pressure relief device
RP	recommended practice

Symbol	Description
B	Plume half-width
$c_{\parallel}$	Entrainment constant associated with the direction parallel to the jet plume
$c_{\perp}$	Entrainment constant associated with the direction perpendicular to the jet plume
g	Gravitational constant
p	Momentum
r	Plume radius
ρ	Density
S	Streamline of the plume
θ	Horizontal angle between the plume and the wind
v, v_{cl}, v_{wind}	Velocity (plume centerline, wind)

This page left blank

1. INTRODUCTION

Hydrogen holds promise as an energy-dense, low-carbon fuel for locomotive applications, but it is also still a rather nascent technology. One important consideration in the hydrogen locomotive industry is how a hydrogen plume would behave as it exits a vent stack, which is a necessary part of the locomotive or tender car design that is used to maintain a safe pressure in the storage vessel by allowing the release of some hydrogen. A second related question of interest is how wind might affect a plume. "Wind" in this context could refer to air flow from any source, including ambient wind or the force on a plume caused by movement of the locomotive. Physics modeling of both these phenomena can lead to insights into the risk profile of a hydrogen-powered locomotive venting system and may potentially reveal gaps where design or protocol changes can be implemented to maintain a safe system.

The Hydrogen Plus Alternative Risk Assessment Models (HyRAM+) v5.1 software contains physics models for buoyant jet plumes of different fuels in a quiescent ambient [1]. Its open-source code allows for the addition of or modification to models as well as the testing of different models in the Python backend. HyRAM+ v5.1 was used to understand how a hydrogen plume is affected by the size of the vent stack, and the implications of physical phenomena like momentum- and buoyancy-driven entrainment on the plume shape and size. It was also used to implement, test, and validate different wind correlations found in literature.

This page left blank

2. MODELING OF A HYDROGEN RELEASE THROUGH A VENT STACK

2.1. Vent Stack Methods

First, a study was conducted to model the shape and size of a plume of vented hydrogen and see how a design choice like the diameter of the vent stack could affect the plume behavior. Many vent stacks, for hydrogen as well as natural gas and other fuels, are designed like the simple schematic shown below in Figure 2-1. This graphic shows how the source of the hydrogen, such as the tank, releases hydrogen directly from a pressure relief device (PRD), into a vent stack that transports the hydrogen to a point above the locomotive or tender car and any ancillary equipment, so the hydrogen does not impinge on anything or accumulate anywhere within the system. While many vent stack designs exist, including angled geometries, this study was conducted under the assumption that the release of hydrogen would be directly vertical. Additionally, the vent stack typically has a larger diameter than the PRD, and is sized so as to limit pressure buildup downstream of the PRD while also preventing back-mixing of the ambient species with the discharged species [2].

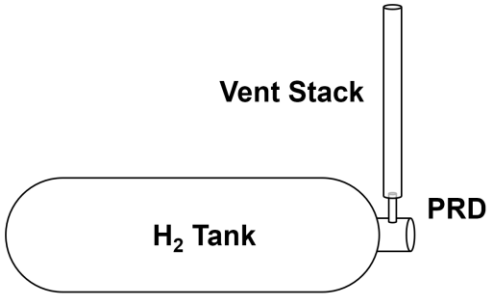


Figure 2-1. Schematic showing simple vent stack model used for the study.

For this study, the release modeling of hydrogen was assumed to happen in two parts. First, the PRD opens into the vent stack. Second, the hydrogen that traveled into the vent stack is released from the opening of the vent stack at the top. Since the physics models in HyRAM+ v5.1 are meant to represent the unconstrained release of hydrogen into open air, they are not appropriate for modeling the movement of hydrogen through the vent stack between the PRD and the open air. Thus, a simplifying assumption was made to equate the mass flow rate out of the vent stack with the mass flow rate out of the PRD. While this assumption may not be a detailed depiction of how hydrogen actually moves through a vent stack, it is likely sufficient for an overall understanding of the hydrogen plume behavior; it would be most accurate for short vent stacks and vent stacks that are not much wider than the PRD orifice. However, the vent stack length was not specified in this problem, and effects of vent stack length such as friction were not considered in the calculations; perfect plug flow of the hydrogen from the PRD through the vent stack was assumed. This model is intended to predict the dispersion of hydrogen in air after the outlet of the vent stack, not to determine the proper size (length or diameter) of the vent stack itself. The hydrogen was assumed to be stored in the tank at 27°C (81°F) and 45 MPa (5426 psi). The PRD was assumed to have a diameter of 6 mm. If the contents of a tank and PRD with these properties were released into ambient air with a temperature of 20°C (68°F) and 0.1 MPa (15 psi), the flow rate would be 750 g/s. Even though this ambient assumption does not exactly reflect the physical mechanism of the PRD discharging directly into a vent stack that is already full of hydrogen, it will still be accurate unless there is significant backpressure in the vent stack; this is because the flow is choked, so the flow rate is only dependent on the conditions upstream of the orifice (i.e., in the tank).

The HyRAM+ v5.1 physics models for jet plumes use pressure-driven flow out of an orifice to compute plume properties. Thus, the backpressure in the vent was empirically determined so that the flow rate out of the vent outlet would be the same as the flow rate into the vent (out of the PRD). Then, the jet plume could be defined by the determined vent pressure, the assumed temperature (20°C, or 68°F), and the assumed ambient conditions. This process was conducted for each vent stack diameter that was tested. The overall modeling process for vent stack releases is shown in Figure 2-2.

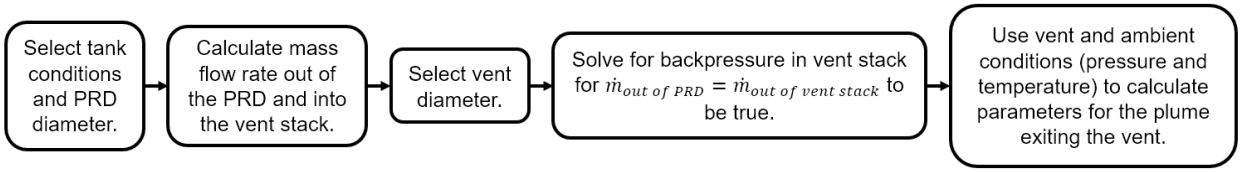


Figure 2-2. Flow chart showing workflow for vent stack calculations.

Figure 2-3 shows the calculated vent pressure required for a vent of each tested diameter to expel 750 g/s of hydrogen at its effluent, to match the vent stack influent (and PRD effluent).

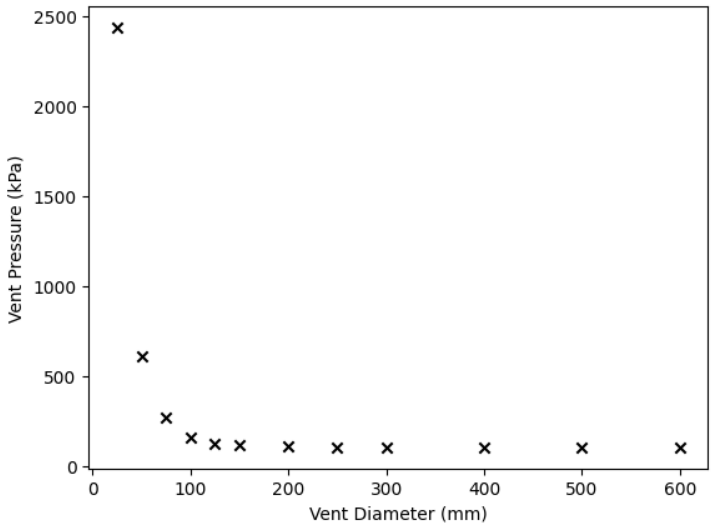


Figure 2-3. Vent pressure required for 750 g/s effluent flow rate for each tested vent diameter.

The vent stack diameter was varied between 25 and 600 mm. While this range includes diameters that are likely much larger than the actual vent stacks for hydrogen locomotives, the objective of the study was to broadly understand how changing this design parameter would affect the plume size and shape.

2.2. Vent Stack Findings

Concentration contours can be used to visualize the shape and size of a hydrogen release into air. Figure 2-4 below shows the 4% mole fraction concentration contours of hydrogen in air, for several vent stack diameters, all from a vertical release with an effluent flow rate of 750 g/s, based on hydrogen storage at 27°C (81°F) and 45 MPa (5426 psi) and released through a PRD diameter of 6 mm.

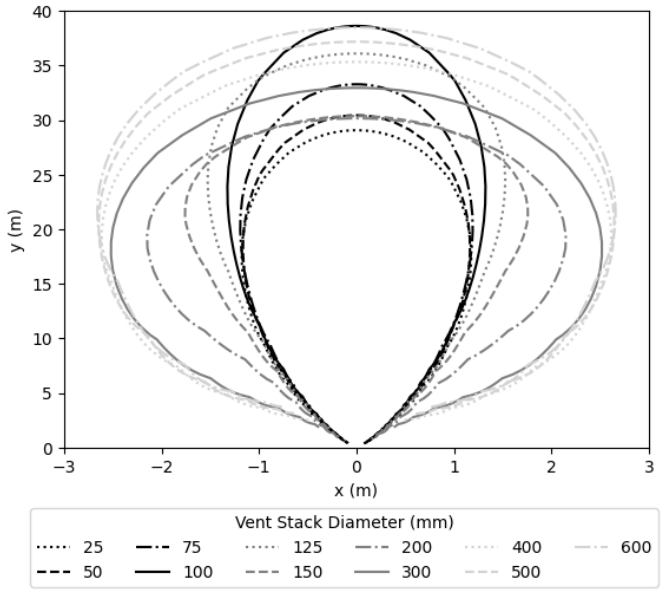


Figure 2-4. Jet plume contours showing 4 mol% concentration of hydrogen for different vent stack diameters for a constant mass flow rate of 750 g/s.

As the vent stack diameter increases from 25 mm to 100 mm, the plume shape first seems to lengthen vertically (axially) and widen (radially) slightly. As the diameter increases between 100, 125, and 150 mm, the plume then begins to shorten vertically and become much wider. Then, as the diameter increases between 150 mm and 600 mm, the plume again lengthens vertically and widens. For the purposes of this report, the plumes were sorted into three sections based on the general shapes and shape trends of the plumes. The first group was made up of the plumes from vent stacks 25 to 100 mm in diameter. The second group was made up of the plumes from vent stacks with diameters between 100 and 150 mm. The final group was made up of the plumes from vent stacks 150 to 600 mm in diameter. The first and third groups were defined by their distinctive shapes (the former having plumes that were axially longer and radially narrower; the latter having plumes that were axially shorter and radially wider). The middle group was considered a transition between the plumes in the other two groups. A similar way of representing this information is by plotting the concentration along the streamline, or centerline, of the plume; this plot is included in Figure 2-5(a) for reference.

The trends in the first and third groups were similar in terms of the lengthening and widening of the 4% contour with increasing vent stack diameter. This result was confounding, since a constant effluent mass flow rate meant that effluent velocity decreased with increasing vent stack diameter, as shown in Figure 2-6. This decreasing effluent velocity would suggest less momentum of the plume at the orifice, so a shorter plume might be expected. A plot of the velocity along the centerline of the plume is also provided in Figure 2-5(b).

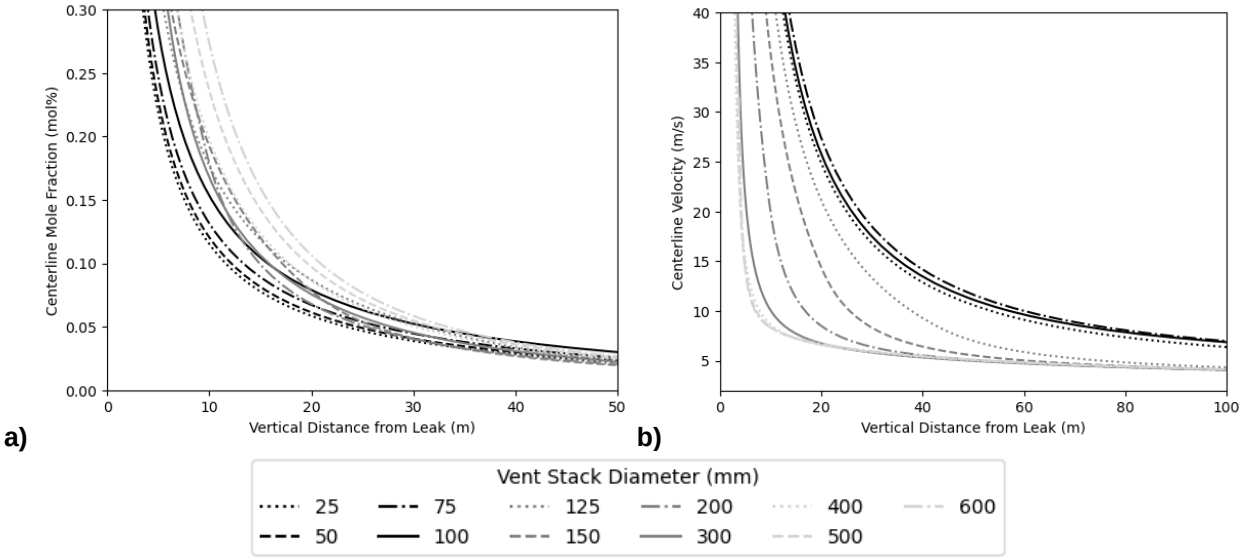


Figure 2-5. a) Centerline mole fraction and b) centerline velocity along the streamline of the plume for different vent stack diameters.

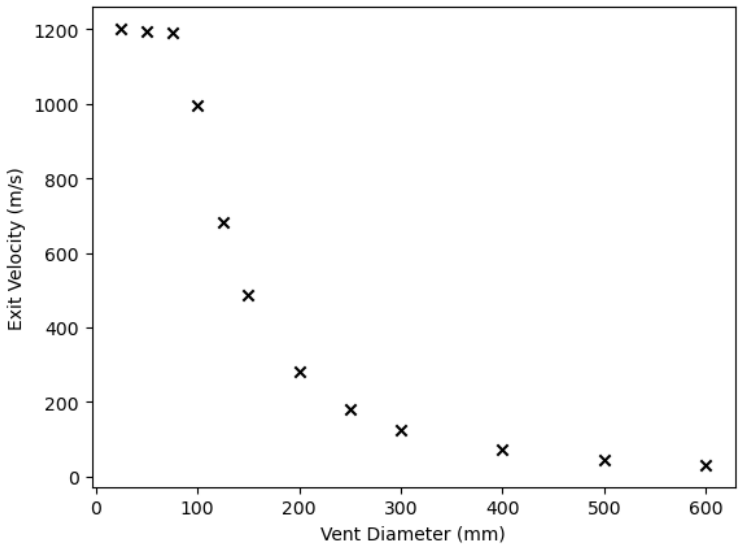


Figure 2-6. Velocity of vent stack effluent as a function of vent diameter for a constant mass flow rate of 750 g/s.

Physical velocity thresholds can provide some explanation as to the reason that, for the conditions used in this study, there is changing behavior between the first group of plumes with diameters up to 100 mm and for the second group of plumes with diameters 100 to 150 mm. The plumes exiting vent stacks with diameters up to 75 mm are all choked flow, which means the exit velocities are equal to the speed of sound for the conditions (temperature, pressure, gas composition) at the vent stack outlet, and that the pressure at the vent outlet is above ambient pressure. The shape and size of these plumes are dependent mostly on the conditions upstream of the vent outlet, such as the temperature and backpressure in the vent. All the other plumes that exit vent stacks with diameters 100 mm and greater are unchoked flow, so the exit velocity is subsonic, the pressure at the vent outlet is ambient, and the shape and size is dependent primarily on the specified mass flow rate.

One of the other important factors affecting the trends in the dispersion profiles is entrainment. Entrainment describes the rate at which the exiting hydrogen mixes with the ambient air; that rate of mixing affects the concentration of hydrogen in air and the shape of the plume. HyRAM+ considers entrainment to be comprised of a momentum-driven and a buoyancy-driven component; these equations and more in-depth descriptions can be found in the HyRAM+ Technical Reference Manual [1]. An overview of these two mechanisms is shown in Table 2-1.

Table 2-1. Summary of entrainment calculations in HyRAM+ v5.1 [1].

	Momentum-Driven Entrainment	**Buoyancy-Driven Entrainment**
Location of Evaluation	At the expanded (atmospheric pressure) orifice, which is the same as vent outlet if unchoked, otherwise after notional nozzle expansion (see HyRAM+ technical reference manual, section 3.2.2 [1])	At multiple points along the jet plume streamline (locations determined by numerical integrator in HyRAM+)
Equation	$E_{mom} = 0.282\left(\frac{\pi d_{exp}^2}{4}\frac{\rho_{exp} v_{exp}^2}{\rho_\infty}\right)^{\frac{1}{2}}$	$E_{buoy} = \frac{a}{Fr_l}(2\pi v_{cl} B)\sin\theta$
Dependencies	• $\boldsymbol{d_{exp}}$: expanded diameter • $\boldsymbol{\rho_{exp}}$: expanded hydrogen density • $\boldsymbol{v_{exp}}$: expanded velocity • $\boldsymbol{\rho_\infty}$: ambient density	• $\boldsymbol{a}$: empirical constant based on densimetric Froude number • $\boldsymbol{Fr_l}$: local Froude number • $\boldsymbol{v_{cl}}$: centerline velocity • $\boldsymbol{B}$: plume radius, or half-width • $\boldsymbol{\theta}$: plume streamline angle

The entrainment model was broken down into several pieces to understand the physical phenomena responsible for the results seen in Figure 2-4. First, momentum- and buoyancy-driven entrainment for each vent diameter were separately plotted in Figure 2-7.

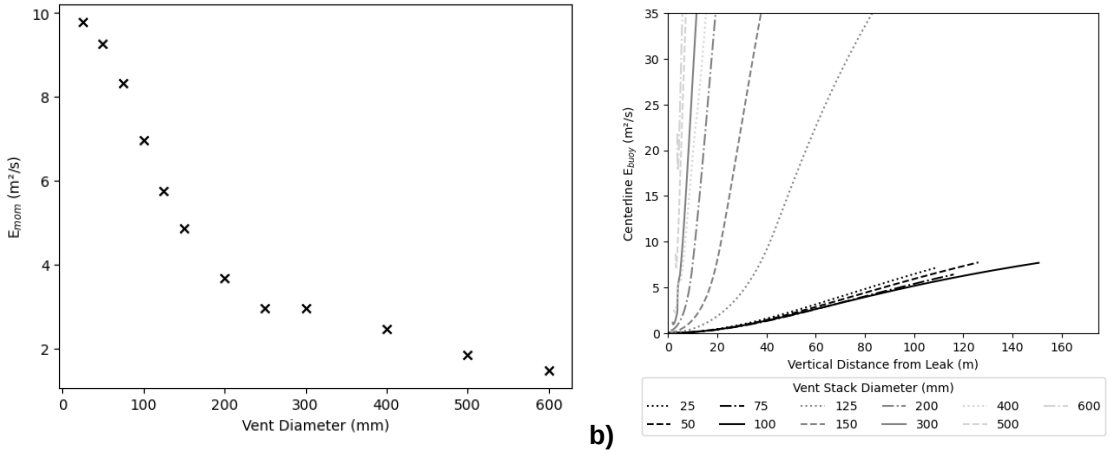


Figure 2-7. a) Momentum-driven entrainment calculated at the expanded orifice and b) buoyancy-driven entrainment calculated along the plume for each vent stack diameter for a constant mass flow rate of 750 g/s.

Figure 2-7(a) shows that, as expected, the momentum-driven entrainment decreases as the vent diameter increases. The combination of the decrease in hydrogen density and velocity at the vent opening leads to the overall decrease in momentum-driven entrainment with the increasing diameter.

Figure 2-7(b) shows that, along each plume, buoyancy-driven entrainment increases along the streamline. This increase happens at a higher rate along the streamline for the higher-velocity cases from vent stacks with diameters up to 100 mm, than for the larger-diameter, lower-velocity, unchoked flow cases. The extent to which each line in the plot extends vertically also reflects the decreasing and increasing plume length trends shown in Figure 2-4. While the momentum-driven entrainment trend is fairly straightforward, the unexpected trends described previously and pictured in Figure 2-4 seem to mirror the trends seen in the buoyancy-driven entrainment plot in Figure 2-7(b). As shown in Table 2-1, buoyancy-driven entrainment is dependent on several parameters, one of which is an empirically derived constant a that depends on the densimetric Froude number based on the piecewise function from the HyRAM+ Technical Reference Manual [1],

$$a = \begin{cases} 17.313 - 0.116665 Fr_{den} + 2.0771 \times 10^{-4} Fr_{den}^2 & Fr_{den} < 268 \\ 0.97 & Fr_{den} \geq 268 \end{cases} \quad \text{Equation 2-1}$$

where the densimetric Froude number Fr_{den} is a ratio of the flow inertia to the forces created by the density difference between the plug flow region directly after the expanded orifice and the ambient air. Since this densimetric Froude number depends on the velocity of the hydrogen out of the expanded orifice, the findings shown in Figure 2-8 are similar to the delineation of flows into choked and unchoked: the flows exiting vent stacks up to 100 mm in diameter are choked and have a Froude number greater than 268 (leading to an a value of 0.97) while the flows exiting vent stacks greater than 100 mm in diameter are unchoked and have a Froude number less than or equal to 268, leading to variable a values based on the Froude number. Thus, there is ample evidence that the flow regimes defined by the flow velocities are responsible for the grouping of plume shapes between flows from vent stacks up to 100 mm and flows from vent stacks larger than 100 mm.

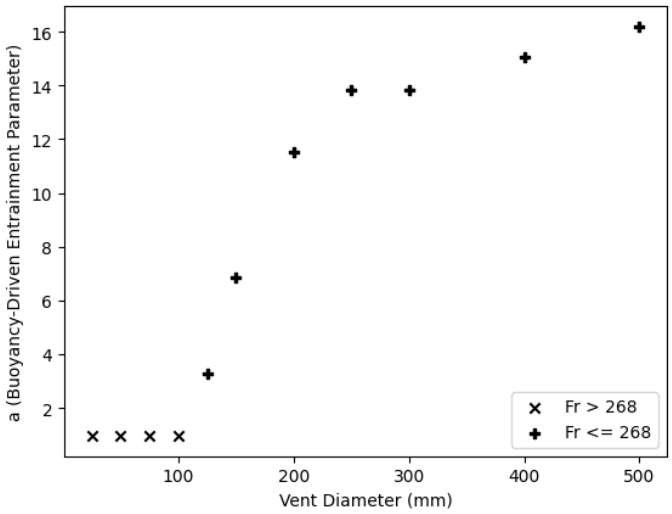


Figure 2-8. Buoyancy-driven entrainment constant a for different vent diameters for a constant mass flow rate of 750 g/s.

The combination of momentum- and buoyancy-driven entrainment can also offer insight into the physical phenomena that lead to the trends in the group of intermediate-sized vent stacks. Table 2-2 below shows momentum-driven entrainment calculated for each vent diameter. Since buoyancy-driven entrainment changes across each plume, the constant entrainment parameter a is shown as an approximate representation of buoyancy-driven entrainment for a whole plume. Additionally, the last column of the table shows the point in the plume when buoyancy begins to dominate entrainment; for most of the cases, momentum starts out dominating the plume entrainment close to the nozzle. These y-positions were determined by calculating momentum-driven entrainment for each overall plume and comparing it to the buoyancy-driven entrainment calculated at each calculation node of the plume model. The location of the node at which the buoyancy-driven entrainment was calculated as higher than the momentum-driven entrainment was noted in the last column of Table 2-2.

Table 2-2. Momentum and buoyancy entrainment observations for each tested vent diameter.

Vent Diameter (mm)	Momentum-Driven Entrainment (m^2/s)	Buoyancy-Driven Entrainment Parameter a	Approximate Y-position when Buoyancy Begins to Dominate Entrainment (m)
25	9.8	0.97	Momentum dominates
50	9.3	0.97	Momentum dominates
75	8.3	0.97	Momentum dominates
100	7.0	0.97	132
125	5.8	3.29	33
150	4.0	6.86	16
200	3.7	11.52	7.5
250	3.0	13.84	4.1
300	3.0	13.84	3.8
400	2.5	15.06	3.0
500	1.9	16.19	Buoyancy dominates
600	1.5	16.67	Buoyancy dominates

The table confirms that for the smaller-diameter high-velocity, high-momentum vents, momentum-driven entrainment dominates at all heights of the plume. As the vents become larger, the buoyancy-driven entrainment begins to dominate overall entrainment closer to the release point; for the two largest tested diameters, buoyancy-driven entrainment dominates the entire plume even close to the release point, since the velocity is so low. The intermediate range of vent stack diameters, from 100 to 150 mm, shows that the dominating entrainment mechanism begins to shift somewhere within the 4 mol% plume contours seen in Figure 2-4, which could be one factor responsible for the different trend within those contours (where the size of the plume decreases with an increasing vent stack diameter).

The open question as yet unexplained by these observations continues to be why the model predicts increasing length of the flammable contour with increasing vent diameter and the associated decrease in velocity. This discrepancy between the expected and observed trends can possibly be explained by the overall entrainment, which is plotted in Figure 2-9. The first group with vent stacks up to and including 100 mm are clearly distinct in the profile of entrainment from the plumes with larger vent diameters. Within this group, as well as separately within the second and third groups, the entrainment decreases with increasing vent diameter. At a functional level, this could mean that lower velocity and entrainment promote less turbulent mixing of hydrogen with air, which means the hydrogen can travel farther from the orifice before being diluted, for larger vent diameters.

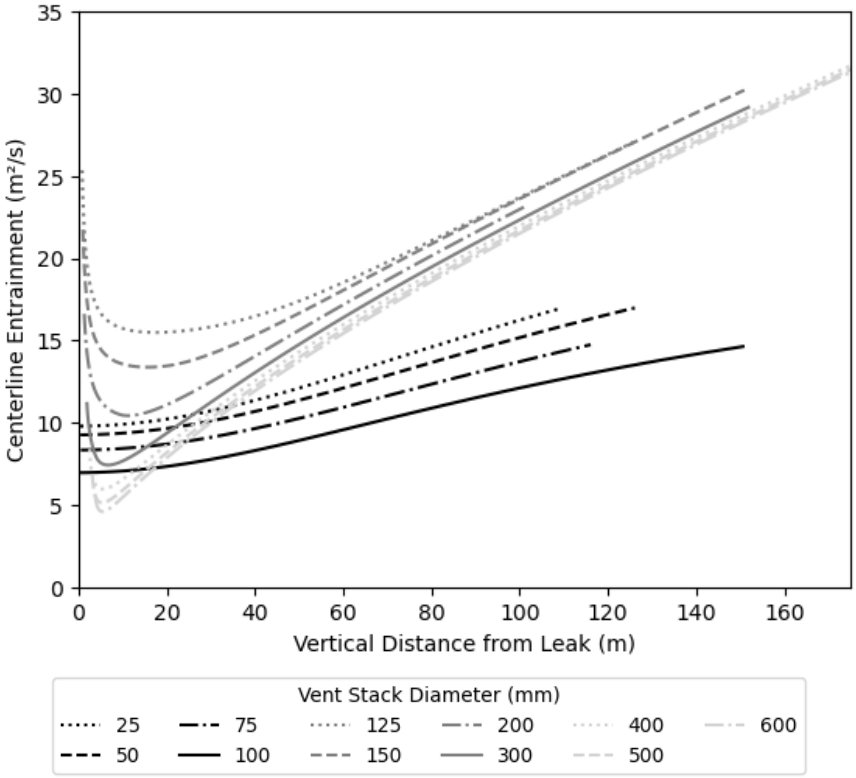


Figure 2-9. Overall entrainment calculated along the plume for each vent diameter.

Different storage conditions can lead to different plume shapes because of the change in mass flow rate through the PRD. In addition to the compressed gas case shown above in Figure 2-4, a subcooled liquid, saturated liquid, and saturated vapor case was tested. The storage conditions are provided in Table 2-3 and a comparison of the vent backpressures required to achieve each PRD mass flow rate is included in Table 2-4.

Table 2-3. Storage conditions for each phase.

Stored Hydrogen Phase	Stored Pressure (kPa | psi)	Stored Temperature (°C | °F)	Calculated Density (kg/m^3)	Mass Flow Rate (kg/s)
Compressed Gas	45000 | 5426	27 | 81	29	0.754
Saturated Vapor	500 | 73	-246 | -411	6	0.032
Saturated Liquid	500 | 73	-246 | -411	61	0.079
Subcooled Liquid	500 | 73	-248 | -415	56	0.139

Table 2-4. Calculated vent pressures in kPa | psi for each vent diameter and storage phase.

Vent Diameter (mm)	Compressed Gas	Saturated Vapor	Saturated Liquid	Subcooled Liquid
25	2,436.644 | 353.4	127.847 | 18.5	258.732 | 37.5	456.071 | 66.1
50	608.006 | 88.2	102.956 | 14.9	111.125 | 16.11	132.179 | 19.2
75	270.131 | 39.2	101.646 | 14.7	103.250 | 15.0	107.322 | 15.6
100	156.985 | 22.8	101.426 | 14.7	101.934 | 14.8	103.217 | 15.0
125	123.657 |17.9	101.366 | 14.7	101.574 | 14.7	102.099 | 14.8
150	112.014 | 16.2	101.345 | 14.7	101.445 | 14.7	101.698 | 14.8
200	104.691 | 15.2	101.331 | 14.7	101.363 | 14.7	101.443 | 14.7
250	102.702 | 14.9	101.328 | 14.7	101.340 | 14.7	101.348 | 14.7
300	101.989 | 14.8	101.326 | 14.7	101.332 | 14.7	101.332 | 14.7

The plumes for the saturated vapor, saturated liquid, and subcooled liquid cases are shown below in Figure 2-10.

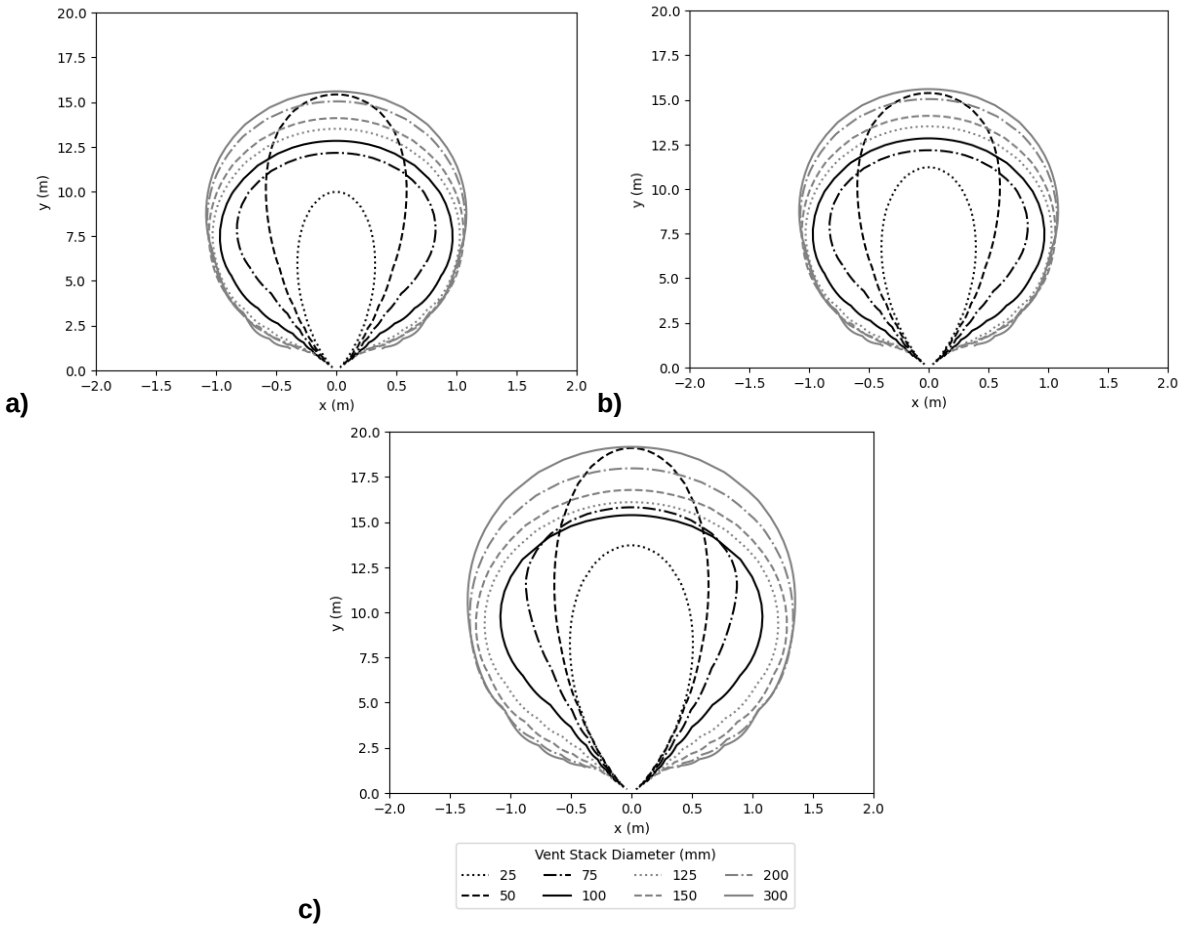


Figure 2-10. Plumes for different vent stack diameters for a) saturated vapor, b) saturated liquid, and c) subcooled liquid storage conditions.

The contours in Figure 2-10 show that stored saturated vapor and saturated liquid lead to similarly-sized plumes – the biggest difference between the two cases occurs with the smallest diameter, where vent backpressure for the saturated liquid case is around twice that of the saturated vapor case, leading to a slightly longer plume from the vent off the saturated liquid storage tank. The plumes from the subcooled vent stack are longer than either of the saturated cases because the mass flow rate out of the PRD is higher. The subcooled vent stack plume is still shorter than the plume from the compressed gas case, which has the highest mass flow rate out of the PRD.

Some differences in the shape and size of the plume out of the vent stack can also be seen when the conditions of hydrogen within the vent stack are varied. Figure 2-11 shows the comparison between the vent stack plume from the compressed gas conditions from the previous examples (27°C, or 81°F, and 45 MPa, or 5426 psi), and a case where the hydrogen is stored as saturated liquid at 0.5 MPa (73 psi), a case where the hydrogen is stored as saturated vapor at 0.5 MPa (73 psi), and a case where the hydrogen is stored as a subcooled liquid at 0.5 MPa (73 psi) and -243°C (-405°F). All these cases use a PRD with a 6 mm diameter and a vent stack with a 25 mm diameter.

As previously mentioned, the model used in this report does not have the capability to predict heating and expansion of the hydrogen as it moves through the vent stack, so three different temperatures at the vent stack exit were assumed. The vent stack temperature was varied between an

ambient 20°C (68°F), a slightly colder -123°C (-190°F), and cryogenic -193°C (-316°F) (note that although this is cryogenic, it is well above the temperature of liquid hydrogen). For ease of comparison, these values are labeled as 293 K, 150 K, and 80 K respectively in the Figure 2-11 plots.

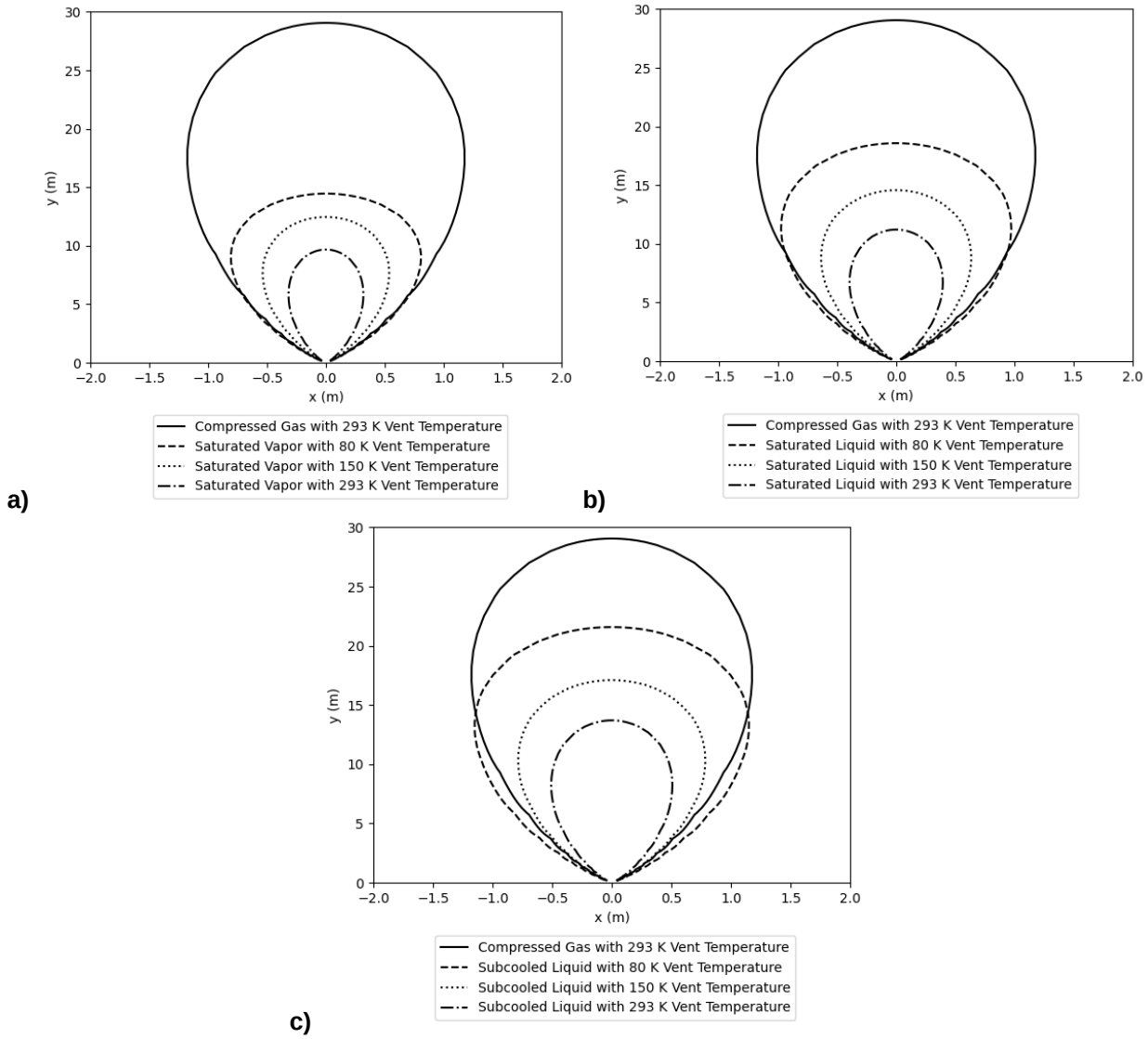


Figure 2-11. 4 mol% hydrogen concentration contours showing the comparison between plumes exiting the vent stack from compressed gaseous hydrogen and a) saturated vapor hydrogen, b) saturated liquid hydrogen, and c) subcooled liquid hydrogen from the tank. All figures show plumes for a 6 mm PRD and a 25 mm vent stack.

For each set of conditions, the contours show, first, that the plume from the compressed gas is larger than the plume from any of the other stored phases. Secondly, for each of the different stored phases, the plume size decreases with increasing vent temperature (in other words, as the vent temperature gets closer to ambient). Between the three stored phases of saturated vapor, saturated liquid, and subcooled liquid, it appears that, for the same vent stack temperature, the subcooled liquid plume is the largest, the saturated liquid plume is the second largest, and the saturated vapor plume is the smallest. Both of these trends are a direct result of the vent backpressures that were calculated for each phase to fulfill the assumption that the mass flow rate out of the PRD and into

the vent stack was the same as the mass flow rate out of the vent stack. The backpressures are plotted over vent temperature for each stored phase in Figure 2-12. The highest backpressure was calculated for the compressed gas, then for the subcooled liquid, saturated liquid, and saturated vapor, respectively. Higher backpressures were required to maintain the mass flow rate assumption for temperatures that were closer to ambient.

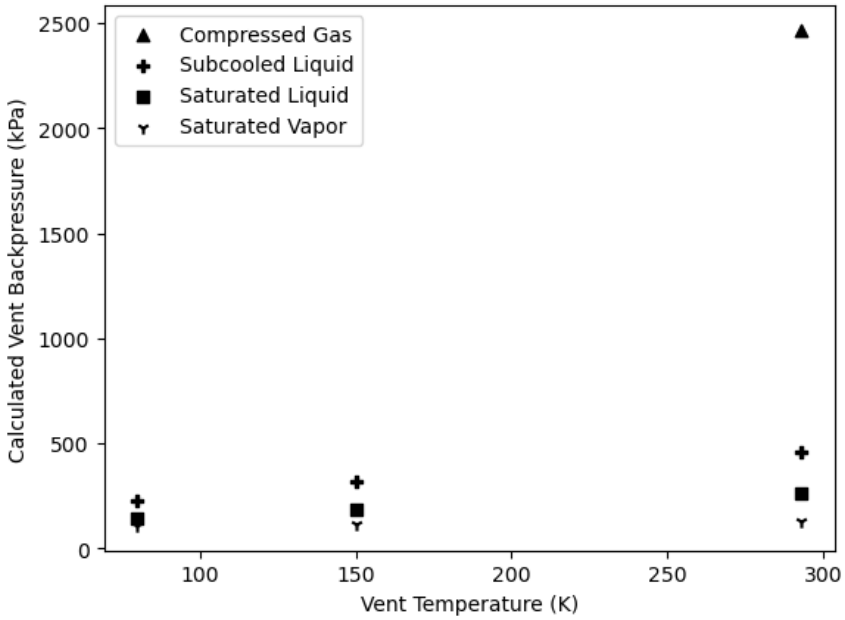


Figure 2-12. Calculated vent backpressures needed at each vent temperature and for each stored phase for the mass flow rate out of the vent to match the mass flow rate out of the PRD and into the vent.

The data from Figure 2-12 is tabulated in Table 2-5.

Table 2-5. Tabulated vent backpressures for each phase and vent temperature.

Stored Hydrogen Phase	Vent Backpressure for 80 K Vent (kPa | psi)	Vent Backpressure for 150 K Vent (kPa | psi)	Vent Backpressure for 293 K Vent (kPa | psi)
Compressed Gas	-	-	2465.196 | 357.5
Subcooled Liquid	225.417 | 32.7	318.310 | 46.2	456.071 |66.1
Saturated Liquid	142.668 | 20.7	181.687 | 26.4	258.732 | 37.5
Saturated Vapor	108.390 | 15.7	114.685 | 16.6	127.848 | 18.5

Table 2-3 shows how the mass flow rate out of the PRD decreases between compressed gas, subcooled liquid, saturated liquid, and saturated vapor conditions. This decrease in mass flow rate follows the same trend of decreasing backpressure in the vent in Table 2-5.

2.3. Vent Stack Model Validation

Using HyRAM+ models to simulate vent stack exhaust requires validation that the models accurately depict experimentally observed behavior. The entrainment models in HyRAM+ are from a paper by Houf and Schefer, which already contains validations of the models against experiments [3]. One main point of comparison, as discussed in the previous section, is the plume length. Figure 2-13 shows the Houf and Schefer model validation against their slow leak experiments; the paper reports a high degree of agreement, within around 6.5% error. The plots suggest that flows with higher densimetric Froude numbers (achieved through higher velocities while keeping diameter constant in these experiments) are longer than flows with lower densimetric Froude numbers. This observation shows the opposite of the trends observed in HyRAM+ in Figure 2-14, where lower densimetric Froude numbers (for larger-diameter, lower-pressure vents) lead to longer plumes.

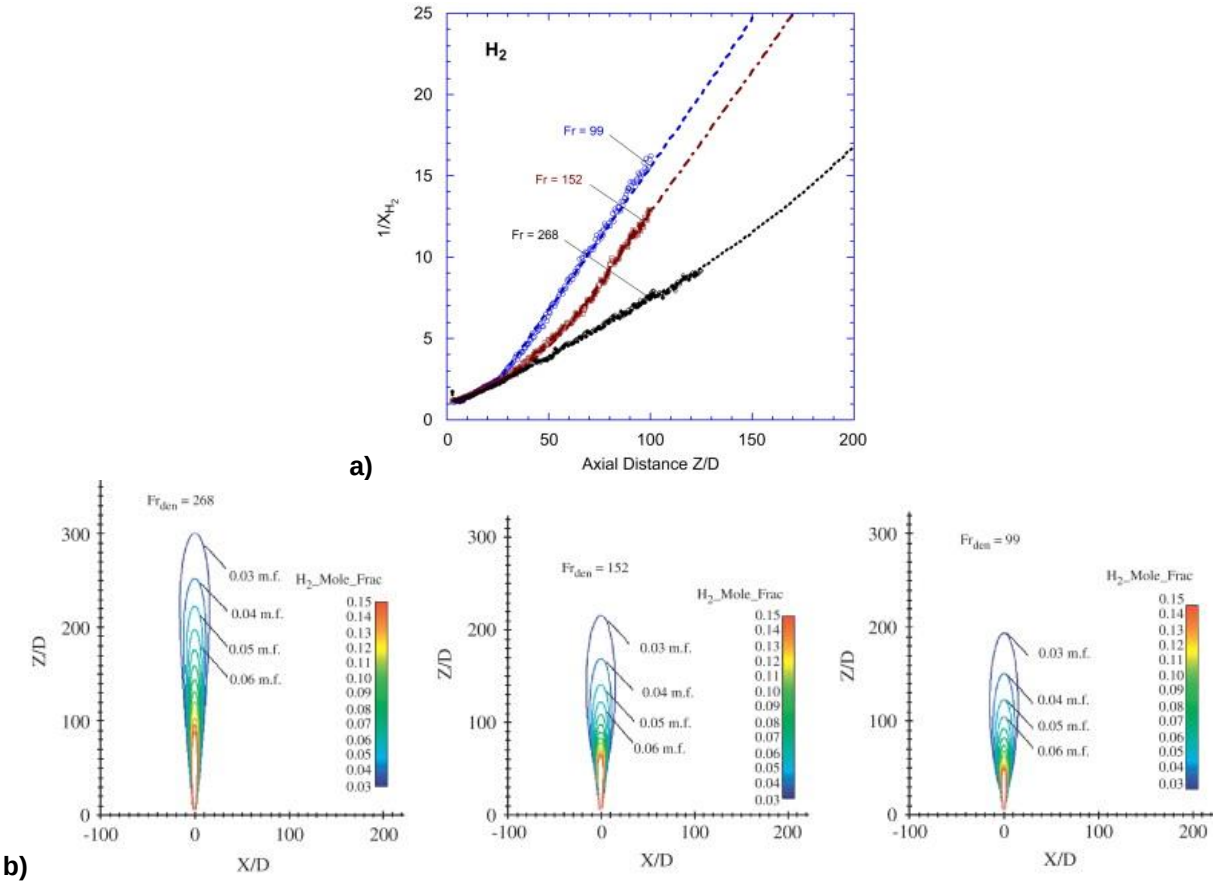


Figure 2-13. a) Simulation-calculated centerline mole concentrations for vertical hydrogen jets (lines) compared to slow leak experimental data (points) and b) simulated plumes out of a 1.905 mm diameter orifice. Figures taken from [3].

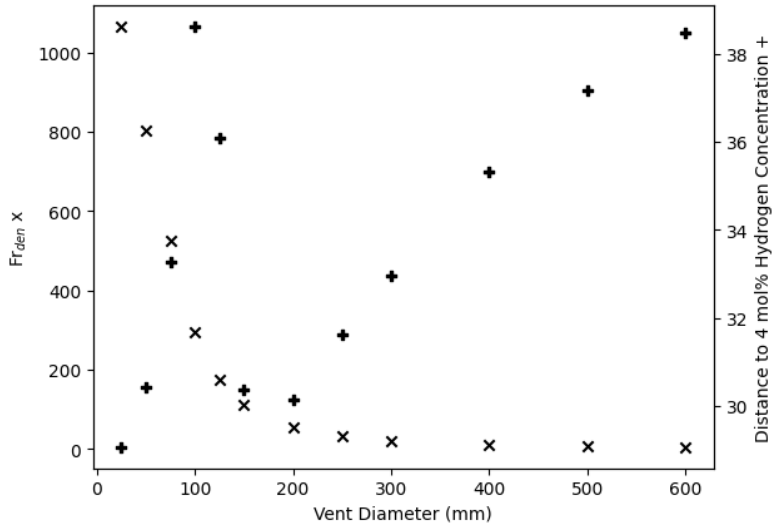


Figure 2-14. Densimetric Froude number and distance to 4% hydrogen concentration for a range of vent diameters for a constant mass flow rate of 750 g/s.

HyRAM+ shows that the Froude number decreases with increasing vent diameter, which is an expected result since velocity decreases with vent diameter to maintain the mass flow rate. However, the trend of centerline distance to the hydrogen flammable concentration with decreasing Froude number is not monotonic. Plumes that are mostly dominated by momentum-driven entrainment (with vent stack diameters around 25-100 mm) or buoyancy-driven entrainment (with vent stack diameters greater than 200 mm) show increasing distance to the hydrogen flammable concentration with decreasing Froude number; the trends within the intermediate plumes experiencing a combination of momentum- and buoyancy-driven entrainment is less clear. The trend of increasing distance to the flammable concentration with decreasing Froude number is the opposite of the trend found in the Houf and Schefer model and shown in Figure 2-13(b). However, the Froude number was changed through different parameters in the HyRAM+ calculation in this report and in the Houf and Schefer paper: in this calculation, the mass flow rate was kept constant while the vent stack diameter was varied, whereas in the Houf and Schefer paper, the orifice diameter was kept constant while the mass flow rate was varied. The parameters between the two experiments are also different, with the HyRAM+ calculations using vent stack diameters 1-2 orders of magnitude larger than the 1.905 mm diameter in the slow leak experiment cited by Houf and Schefer.

HyRAM+ has been validated in the past against other experiments [4], such as the small-orifice experiments described in a paper by Han et al. [5]. In this paper, hydrogen mole fractions are measured within a plume exiting a high-pressure leak. The experimental results plotted against simulations provided in the paper are shown in Figure 2-15; for each pressure, the results indicate that larger diameter leaks have longer plumes. A comparison cannot be directly made between the results of the simulations presented in this report and the experimental data in the Han paper, since the experimental data relied on experiments in which only the diameter varied while the backpressure remained steady (which would lead to a different mass flow rate in each case), whereas the modeling done for this report varied the diameter and backpressure in order to keep the mass flow rate constant across all scenarios. Additionally, the Han paper shows results for horizontal plumes and orifices less than 1 mm in diameter, which are both conditions that do not reflect the scenarios evaluated in HyRAM+ for this paper.

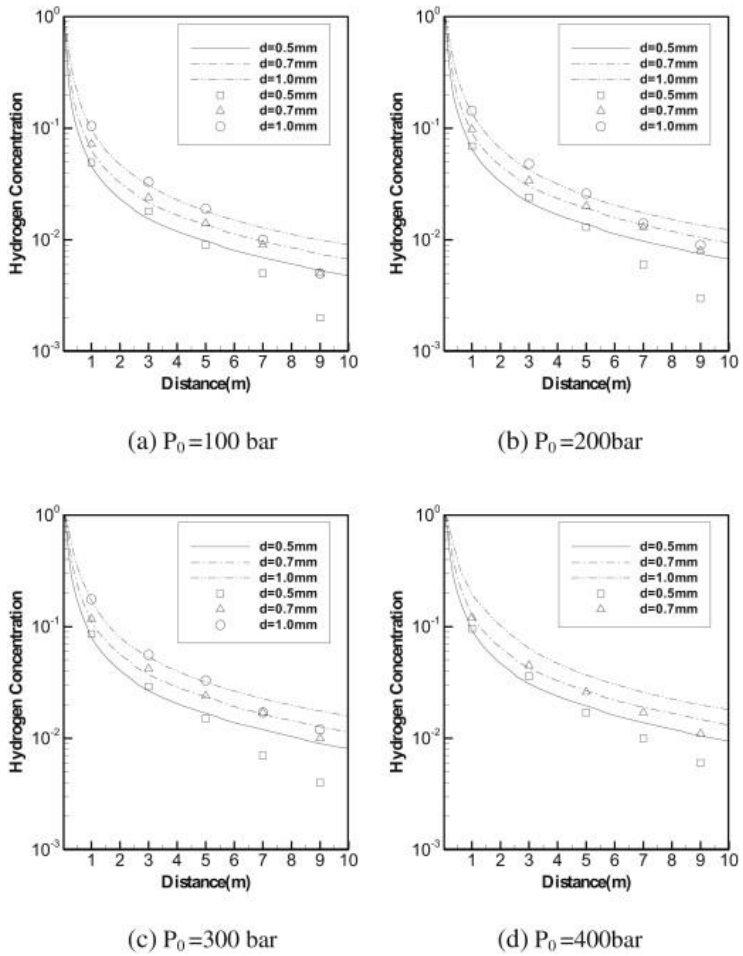


Figure 2-15. Simulation-calculated centerline mole concentrations for horizontal jets (lines) compared to experimental data (points). Figures taken from [5].

Besides modeling the way a jet plume forms in air once hydrogen exits a vent stack, it is also important to use experimental data to understand how to accurately model the movement of hydrogen through the vent stack itself. As previously mentioned, the calculations in this report were conducted under the assumption that the hydrogen moves as a plug with constant density through the vent stack, once it expands within the vent stack after exiting the PRD. Because of this assumption, the vent stack effluent flow could be modeled as having the same mass flow rate as the PRD effluent flow. In reality, there may be a density gradient along the length of the vent stack, which may be affected by the length and diameter of the vent stack as well as the differences between the conditions in the tank such as pressure and temperature. As mentioned earlier, this gradient may be negligible for very high pressure and velocity cases, and for shorter vent stacks. Nevertheless, it would be worthwhile to understand the behavior of the hydrogen in the vent stack itself. HyRAM+ is meant for analyzing hydrogen releases into the open air and does not currently have the capability to analyze the flow of hydrogen through a vent stack, but using a tool such as computational fluid dynamics could be an appropriate option for conducting this analysis.

Additionally, it would be helpful to have experimental data to observe the behavior of hydrogen through a vent stack, including aspects like the heating up and/or expansion of the hydrogen as it travels through. Observations of trends for this behavior with respect to vent stack design choices such as length and diameter would also provide insightful information. Trends could be used to

make assumptions – such as the plug flow assumption made in this report – and use HyRAM+ results as a fairly good representation of this situation.

Researchers at Sandia National Laboratories and Lawrence Livermore National Laboratory conducted experiments on the behavior of cryogenic hydrogen out of vent stacks [6]. The emphasis of the study was on the behavior of the plume in the open air and not as much the behavior within the vent stack. Still, the results of the experiment are relevant to the topic of this report because they show, first, that the HyRAM+ plumes qualitatively match the shape of the observed plumes. The quantitative results or usage of the paper for validation of the HyRAM+ models is still in progress. Secondly, for cryogenic hydrogen in particular, the experiments show that the hydrogen heats up to well above saturation temperature by the time it reaches the end of the vent stack, meaning that it is fully vaporized though still cold, and that it is likely a reasonable assumption to model the plume coming from the vent exit as a cold gas, as is done in this report, rather than a subcooled liquid.

This page left blank

3. MODELING OF A JET PLUME IN WIND

3.1. Wind Modeling Methods

HyRAM+ v5.1 does not have the capability to include wind in the modeling of an unignited jet plume. It does have the capability to include wind in a single direction (horizontal) when modeling an ignited jet flame, but, as this capability was not sufficient for the purposes of this study, as it is not implemented for unignited jets, nor does it consider other wind directions or the effect of wind on mixing with the jet.

In this study, wind was considered to affect the jet plume model in two ways. First, it was expected to have an impact on the momentum governing equation of the plume, by applying force to the plume in the direction of the wind. The non-wind momentum governing equations currently in HyRAM+ and the momentum governing equations that incorporate wind and that were used in this study are shown in Table 3-1.

Table 3-1. Summary of 2D momentum equations adjusted to account for wind.

Parameter	Momentum (x-direction)	Momentum (y-direction)
Base Model (HyRAM+ v5.1 [1])	$\frac{d}{dS}\int_0^\infty (\rho v^2 \cos\theta) 2\pi r dr = 0$	$\frac{d}{dS}\int_0^\infty (\rho v^2 sin\theta) r dr = \int_0^\infty (\rho_{ambient} - \rho) g r dr$
Modified Model	$\frac{d}{dS}\int_0^\infty (\rho v^2 \cos\theta) 2\pi r dr = \boldsymbol{p_{wind,\,x}}$	$\frac{d}{dS}\int_0^\infty (\rho v^2 sin\theta) r dr = \int_0^\infty (\rho_{ambient} - \rho) g r dr + \boldsymbol{p_{wind,\,y}}$
Model Details	$p_{wind,\,x} = v_{wind} \cos(\theta_{wind})\, \rho_{ambient} E$	$p_{wind,\,y} = v_{wind} \sin(\theta_{wind})\, \rho_{ambient} E$

Second, wind was expected to affect the entrainment of air into the plume, which would in turn affect parameters such as the shape and size of the plume. Currently, HyRAM+ calculates entrainment as the sum of a momentum-driven component and a buoyancy-driven component; these two terms depend on different parameters and are computed separately, as shown in Table 2-1. The Gaussian jet plume characteristics such as centerline velocity and density and half-width, or radius, of the plume are calculated at multiple nodes along the streamline. For the first entrainment model tested in this study, entrainment was assumed to have a third, independently calculated wind-driven term included in it, as shown in Equation 3-1.

$$E = E_{momentum} + E_{buoy} + E_{wind} \qquad \text{Equation 3-1}$$

The wind-driven entrainment (E_{wind}) was calculated using the relationship,

$$E_{wind} = B(c_\perp \left| v_{wind} sin\left(\theta_{jet} - \theta_{wind}\right)\right| + c_\parallel \left| v_{wind} cos\left(\theta_{jet} - \theta_{wind}\right) - v_{cl,plume}\right|). \qquad \text{Equation 3-2}$$

Equation 3-2 was a hypothesis for how wind might impact entrainment. Entrainment is the phenomenon through which the hydrogen mixes turbulently with air and consequently gets diluted. The relationship shown above shows entrainment affecting the plume in two directions: the direction perpendicular to the plume streamline at any given node, and the direction parallel to the streamline. Both components depend on the relative angle of the wind to the jet and the velocity of the wind; for the parallel component, this velocity is computed as the velocity of the wind relative to the centerline velocity of the plume, so as not to double-count effects of the plume's own movement on its behavior. Each term in Equation 3-2 is also multiplied by a coefficient associated with the corresponding direction; since this is a generic relationship, these coefficients would ideally

be found experimentally and incorporated into the full hydrogen-specific wind-driven entrainment correlation. Finally, entrainment is proportional to the half-width B; entrainment happens on the periphery of the jet and is therefore likely proportional to the circumference at each node.

It was assumed that the wind profile was constant across the space occupied by the jet plume of interest. Realistically, the direction or speed of the wind may differ with height off the ground, but these more complex wind profiles were not considered in this implementation of the wind entrainment model.

3.2. Wind Modeling Literature Search

As mentioned in the previous section, the hypothesized wind entrainment model shown in Equation 3-2 contains two unknown coefficients related to the wind-driven component of entrainment. To empirically determine optimal values for these parameters, a literature search was conducted to find any published experimental data on the behavior of hydrogen plumes in wind. The HyRAM+ v5.1 unignited jet plume model was already validated for the case of a quiescent ambient [4], so the focus in this study would be the contribution of wind to the entrainment model.

Several papers provide their own models for general plume dispersion, often with validation against experiments. For example, Gebhart et al. published different generic models for the behavior of buoyant momentum jet plumes, which are meant to be used for a variety of different scenarios such as discharge of cooling water into a different temperature body of water, discharge from a condenser on a moving ship, and hot gas from a vent stack or gas turbine exhaust pipe [7]. Many of the models provided in Gebhart et al. are customizable for different types of gases or particulates using empirical constants that are tuned or require tuning to experimental data. The Gebhart et al. models consider the discharge of a jet plume into different flows such as cross-flow, co-flow, and counter-flow, but they are not wind specific, as the scenarios in question are not all confined to gaseous media. Zhang and Ghoniem also developed a model for wind-blown, buoyancy-driven plumes, mostly in the context of smoke from oil spill fires, forest fires, large-scale explosions, and hot exhaust plumes from industrial stacks [8]. A paper by Dürig et al. provided models of the movement of ash particulate matter from volcanic plumes in wind, using data from volcanic events for validation [9]. Shu et al. modeled liquid hydrogen spills and validated the model using spilled liquid helium experiments and controlled wind within a confined cabin [10]. The American Petroleum Institute published Recommended Practice 521, the Guide for Pressure-Relieving and Depressuring Systems, which contains information about the shapes of petroleum gas vent stack plumes in the presence of cross-flow [11]. The Areal Locations of Hazardous Atmospheres (ALOHA) model [12] published by the U.S. EPA can also be used to model flammable gas clouds in variable wind environments, but only provides very conservative one-dimensional (overhead) concentration information, rather than accounting for buoyancy and non-ideal effects that may be present with high pressure or low temperature hydrogen.

It is evident that there is existing knowledge on the behavior of dispersing jet plumes in a non-quiescent ambient, and data as well as qualitative observations form buoyant plumes in wind from non-hydrogen sources can be generally helpful in understanding the behavior of buoyant plumes. Many of the mentioned models such as the Zhang and Ghoniem and Dürig et al. papers do not model a plume being released from a specific point – unlike the jet plume models in HyRAM+, there is no orifice, nor is there a momentum-driven component. The movement of a fuel through the orifice in HyRAM+ largely affects the properties and behavior of the plume, and the HyRAM+ models were validated against the case of momentum-driven jet plumes out of an orifice rather than

against purely buoyancy-driven dispersion of an existing cloud. These physical mechanisms may mean that it would not be possible nor helpful to use these papers for any sort of quantitative comparison to the results in HyRAM+. Knowing about the discharging behavior of other buoyant, non-hydrogen fluids or particulates can clarify how hydrogen plume behavior compares to the releases of other fuels or chemicals into the air. Ultimately, however, hydrogen-specific data is required to ensure that the models used to simulate hydrogen plumes are at least somewhat accurately predicting its physical behavior.

Some experiments have been done within the topic of hydrogen releases into a non-quiescent ambient. Witcofski and Chirivella conducted a liquid hydrogen spill outdoors and used temperature data to determine the corresponding hydrogen concentration contours [13]. Like some of the non-hydrogen studies discussed earlier, these spilled experiments may provide some indication of the buoyant behavior of hydrogen in the presence of wind, but the differences between the liquid pooling scenarios and the scenarios of the jet plume exiting an orifice driven by momentum as well as buoyancy may be physically different enough that it would not make sense to use these experiments for model validation. A paper by Buttner et al. analyzes experiments performed outdoors in which liquid hydrogen was released through an orifice [14]. However, when experiments are done outdoors, there is little control over the conditions of the ambient air into which the hydrogen is being discharged. Therefore, the wind speeds and directions may be variable both temporally and spatially, and those nuances may not always be captured by the few locations at which measurements of the ambient conditions are taken. Variabilities across space in parameters such as the wind velocity and direction may also lead to noisier data than what could be collected in a more controlled experiment like in the Shu et al. paper. Additionally, when releases are unconfined, it is more difficult to tell if the experiments reached a steady state; if they did not, it might not be accurate to fit the HyRAM+ models to those data, as HyRAM+ models steady-state jet plumes (with temporal modeling possible by assuming pseudo-steady-state jet plumes are formed).

The most relevant data found during this literature search was in a paper by Grune et al., which provides some plume concentration data for experimental steady state hydrogen releases from an orifice, within a test vessel [15]. Fans were used to force ventilation in specific directions and velocities. The data from this paper were used to determine optimal coefficients for the wind-driven entrainment correlation, although some assumptions were still required to match the two. For example, HyRAM+ requires inputs including orifice size and backpressure upstream of the orifice. The Grune et al. paper provided an orifice size and a pressure "close to the nozzle" as well as pressures at various points in the experimental setup upstream of the orifice. Because the setup may not be precisely consistent with the physics models upon which the HyRAM+ calculations are based, it was decided that a backpressure in HyRAM+ would be back calculated to match the mass flow rate from the Grune et al. paper, which is a more important parameter in determining the size and shape of the plume. The test matrix and conditions are provided in Table 3-2.

Table 3-2. Conditions for data used from Grune et al. [15]. The ambient conditions were 20°C (68°F) and 101 kPa (14.7 psi) for all cases.

Mass Flow Rate (g/s)	Orifice Size (mm)	Hydrogen Temperature (°C | °F)	Hydrogen Pressure (kPa | psi)	Wind Direction with Respect to Jet	Wind Speed (m/s)
1	1	20 | 68	2043 | 296	Counter	1.5
					3.5
				Co	1.5
					3.5
					5
1	4	20 | 68	140 | 20	Counter	1.5
					3.5
				Co	1.5
					3.5
					5
5	1	20 | 68	10303 | 1494	Counter	1.5
					3.5
				Co	1.5
					3.5
					5
5	4	20 | 68	637 | 92	Counter	1.5
					3.5
				Co	1.5
					3.5
					5

3.3. Wind Modeling Results

Fitting constants of 0.149 for $c_{\parallel}$ and 0.00864 for $c_{\perp}$ were selected; these constants could be optimized in future work. The values of the HyRAM+ predictions compared to the Grune et al. [15] data are shown in Figure 3-1.

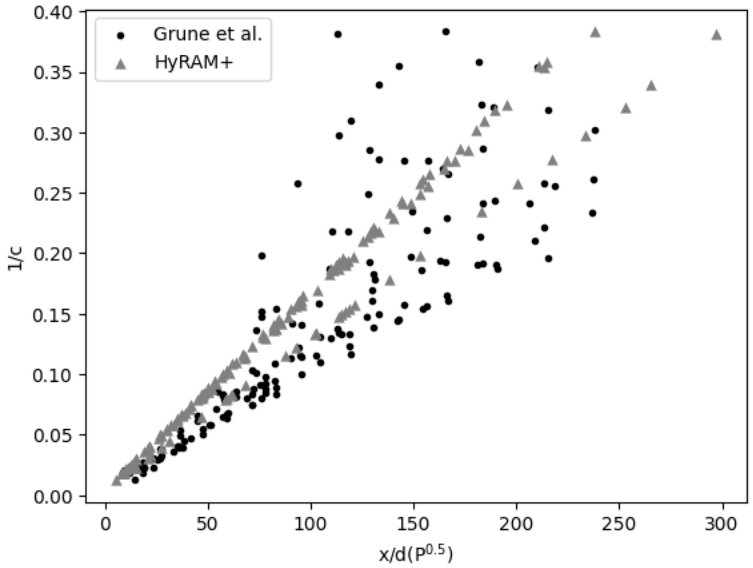


Figure 3-1. Comparison of HyRAM+ data to Grune et al. [15] data using entrainment coefficients of 0.149 for $c_{\parallel}$ and 0.00864 for $c_{\perp}$.

On the axes, c is concentration in mol%, x is distance along the centerline in mm, d is the orifice diameter in mm, and P is backpressure in bar. With the current coefficients for parallel and perpendicular wind entrainment, the R^2 value is 47%. In future work, these coefficients could be tuned to the full set of Grune et al. [15] data to determine optimal coefficients based on experimental observation.

Mole fraction contours of the plumes in different wind conditions, using the selected wind entrainment constant values from above, are shown in the following figures. Figure 3-2 and Figure 3-3 show how the contour shapes change with different wind angles for a vertical and horizontal release, respectively. Figure 3-6 and Figure 3-7 show how the contour shapes change with different wind speeds parallel to the jet plume for a vertical and horizontal release, respectively. While the wind entrainment model is set up so that it should work with any jet plume and wind direction, this assumption requires validation from experimental data with different jet plume angles.

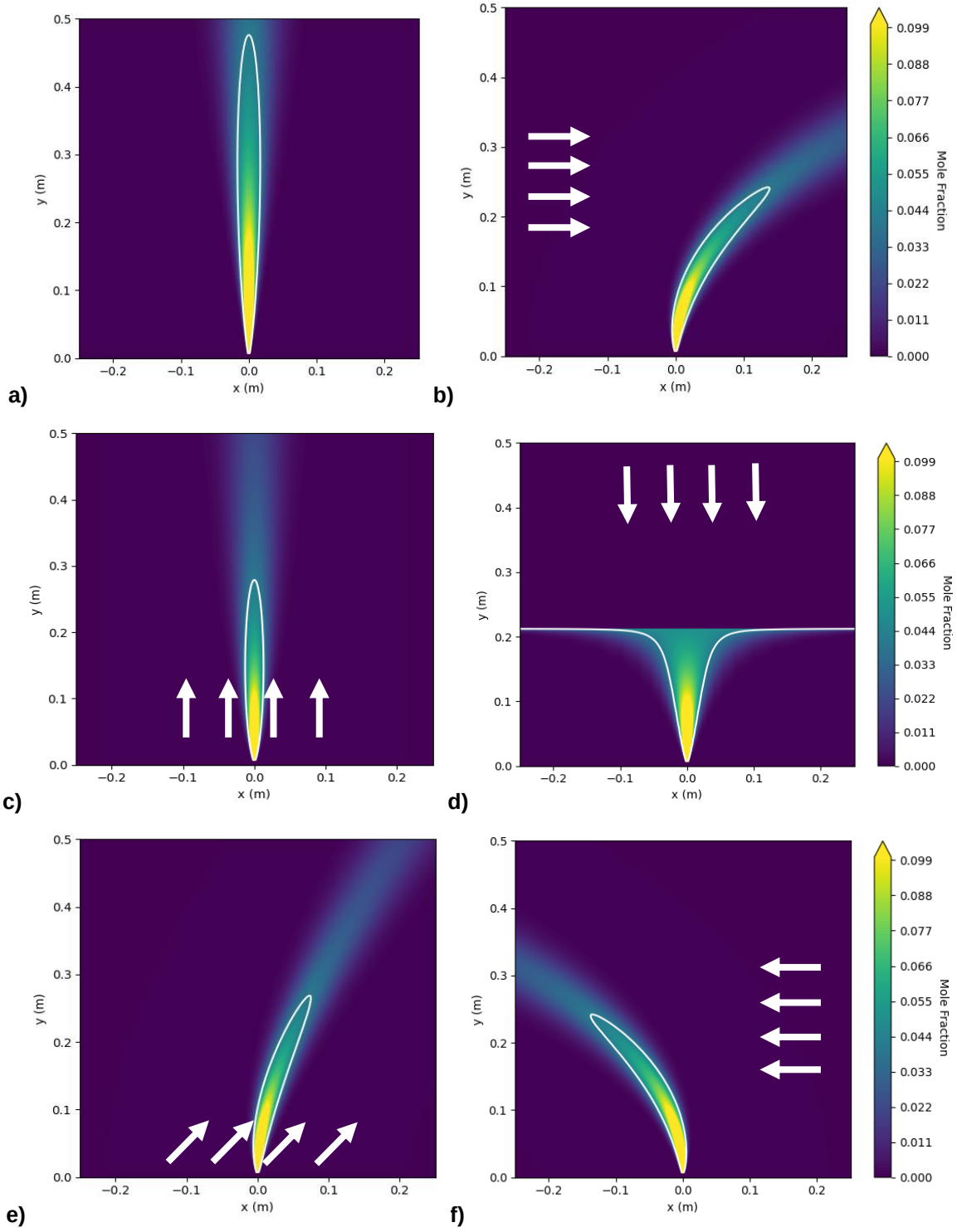


Figure 3-2. 4 mol% hydrogen concentration contours using HyRAM+ wind entrainment model, for hydrogen stored at 0.3 MPa (43 psi) and 25°C (77°F), released vertically through a 1 mm orifice, and subject to a) no wind, b) 10 m/s wind at a 0° angle, c) 10 m/s wind at a 90° angle, d) 10 m/s wind at a 270° angle, e) 10 m/s wind at a 45° angle, and f) 10 m/s wind at a 180° angle.

Figure 3-2 shows the behavior of the plume when encountering different wind directions. The directions in which the plume bends are generally intuitive, with the plume bending in the same direction as the 90°, 45°, and 180° winds in Figure 3-2(b), (e), and (f) respectively. In all the wind cases the plume appears to be becoming shorter than the plume in the no-wind case; this observation is especially apparent in the 90° wind case in Figure 3-2(c). This trend was seen in the Grune et al. data: for each set of conditions, adding wind led to shorter plumes. This change in plume length observed in the data was especially apparent for co-flow cases, and less apparent for counter-flow cases. Physically, this trend could possibly be explained by the increased entrainment from wind leading to more turbulent mixing of the hydrogen into the air and consequently faster dilution and dispersion. Figure 3-2(d) shows the HyRAM+ prediction of the plume when experiencing counter-flow, and the flammable contour is very different from the other plume shapes; the plume seemingly hits an invisible wall. The irregularity of the shape is likely due to the difficulty of solving for a changing of directions of a plume in HyRAM+; past studies in HyRAM+ for downward-facing plumes that eventually turn upwards have also been observed as having unintuitive or unrealistic contours.

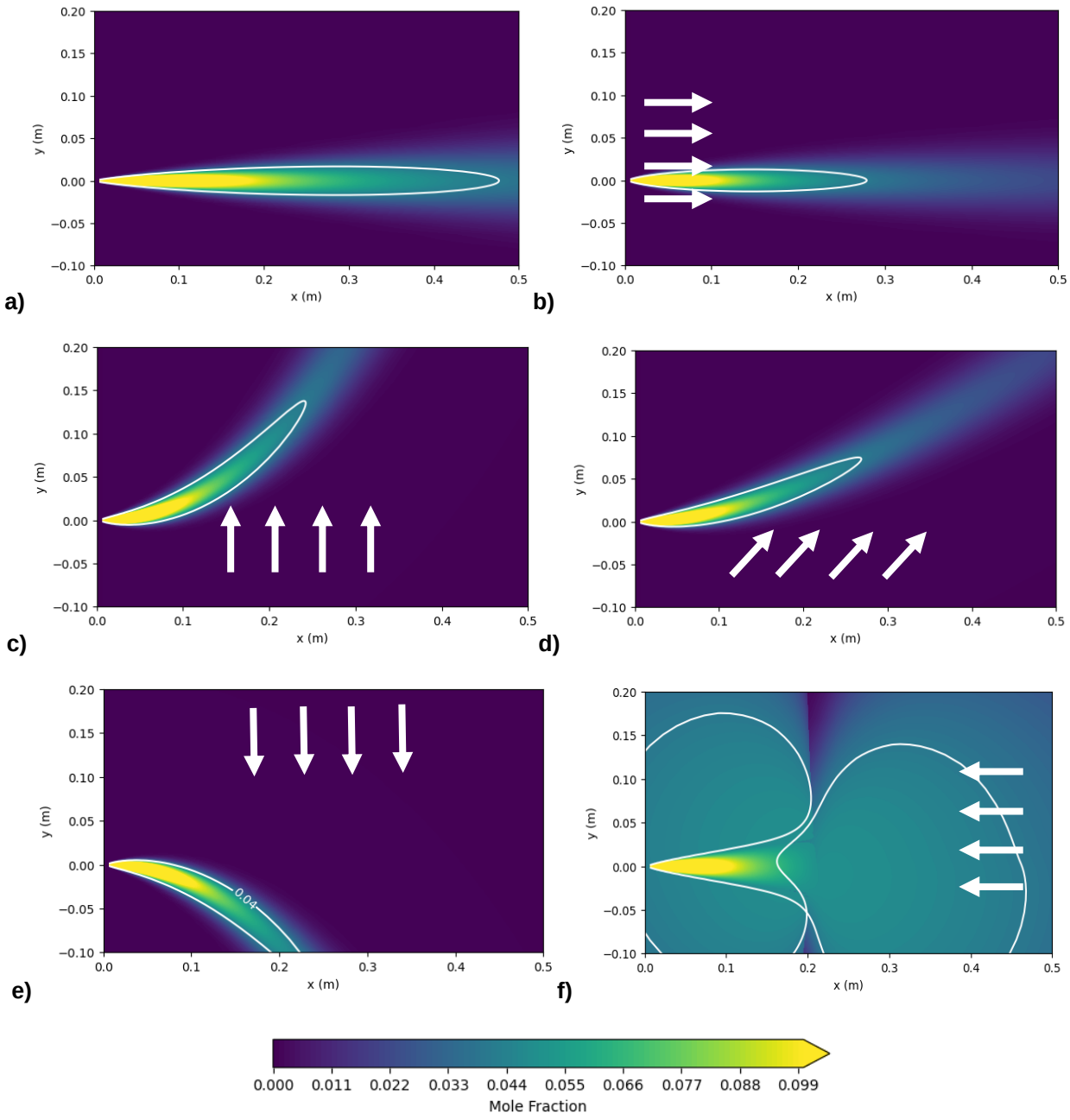


Figure 3-3. 4 mol% hydrogen concentration contours using HyRAM+ wind entrainment model, for hydrogen stored at 0.3 MPa (43 psi) and 25°C (77°F), released horizontally through a 1 mm orifice, and subject to a) no wind, b) 10 m/s wind at a 0° angle, c) 10 m/s wind at a 90° angle, d) 10 m/s wind at a 270° angle, e) 10 m/s wind at a 45° angle, and f) 10 m/s wind at a 180° angle.

Similar trends are observed in Figure 3-3 for a horizontally discharged hydrogen jet: the plume is shortened by the presence of the wind in all cases of a non-quiescent ambient. The mole fraction contour for the counter-flow case in Figure 3-3(f) shows a strange visual representation of the plume nearly changing horizontal direction at approximately 0.2 m. The bulging 4% concentration contour between 0.2 and 0.5 m is likely an artifact of the visualization and not representative of flammable mass being present at that distance.

Investigating the plume and entrainment response to the counter-flowing ambient conditions in more detail indicates how the HyRAM+ prediction handles this scenario. Figure 3-4 shows a 5 m/s counter-flowing wind for a vertical release (note that this is different than the 10 m/s wind in Figure 3-2), showing a rapid end of the flammable contour as the plume half-width and consequently the wind entrainment increases dramatically. Equation 3-2 shows that wind driven entrainment is proportional to the half-width; the increasing entrainment causes the half-width to expand, which consequently causes the wind-driven entrainment to increase in a feedback cycle.

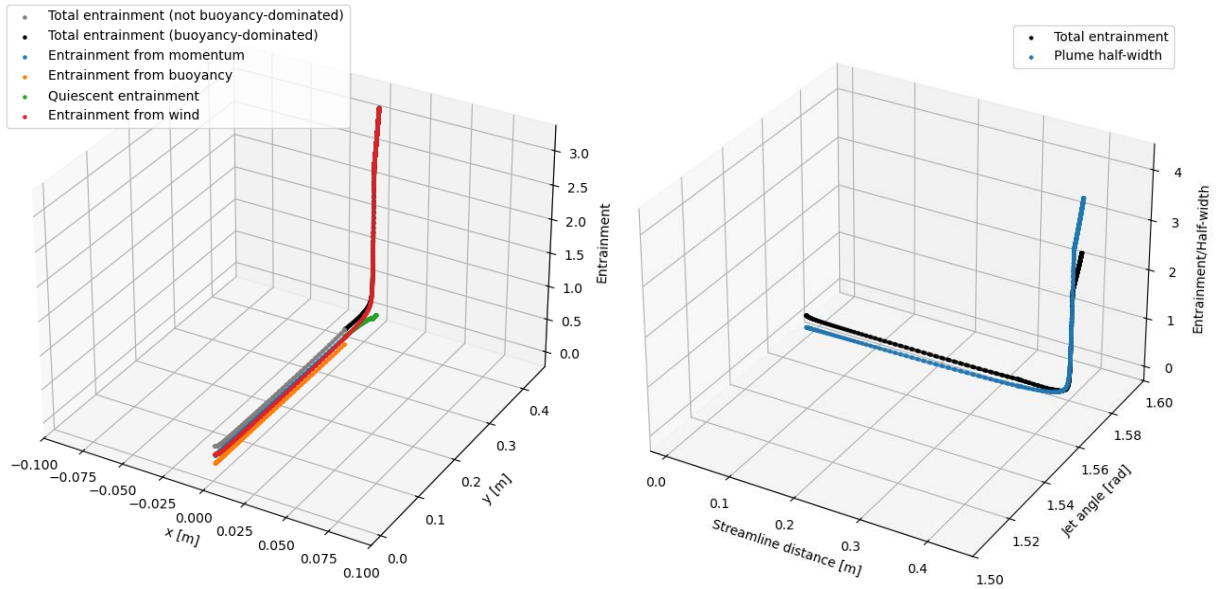


Figure 3-4. HyRAM+ wind entrainment model behavior for 5 m/s vertically counter-flowing wind for a vertical release, showing a) contributions of different entrainment sources, b) overlay of the entrainment and the plume half-width.

Figure 3-5 shows a 10 m/s counter-flowing wind for a horizontal release. Here, the plume trajectory nearly switches directions (the x coordinate) to be coflowing with the wind (note that the vertical distance, y, is very small in the figure). In the middle of the turn, the entrainment is buoyancy dominated (as indicated by the "total entrainment" marker turning from gray to black), with the entrainment peaking, followed by a rapid decrease before a second sharp peak, with a final slow increase as the plume travels in the negative x-direction. The peaks are likely due to the parallel wind entrainment coefficient term being over an order of magnitude larger than the perpendicular term, making counterflow and co-flow have much stronger entrainment than crossflow, which occurs as the plume changes direction.

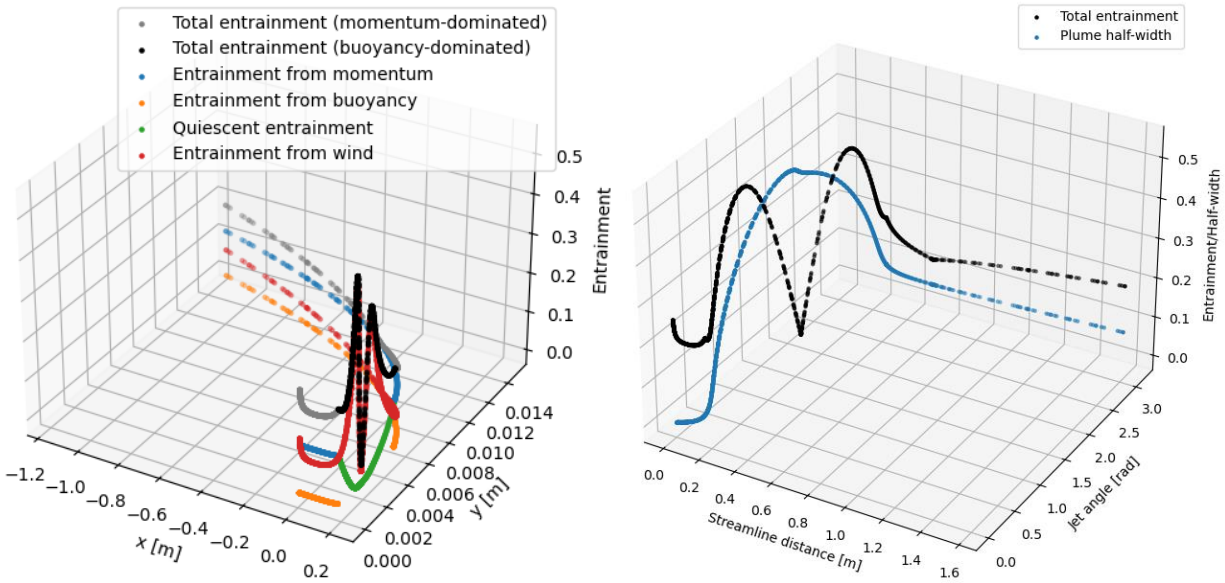


Figure 3-5. HyRAM+ wind entrainment model behavior for 10 m/s horizontally counter-flowing wind for a horizontal release, showing a) contributions of different entrainment sources, b) overlay of the entrainment and the plume half-width.

Despite the possibly unrealistic depiction of the overall hydrogen plume contour in a counter-flowing ambient, the model seems to behave up to the point at which the force of wind is balanced with the force of the plume. Reasonable agreement in Figure 3-1 to data with counter-flow wind would also indicate that the model is functioning correctly.

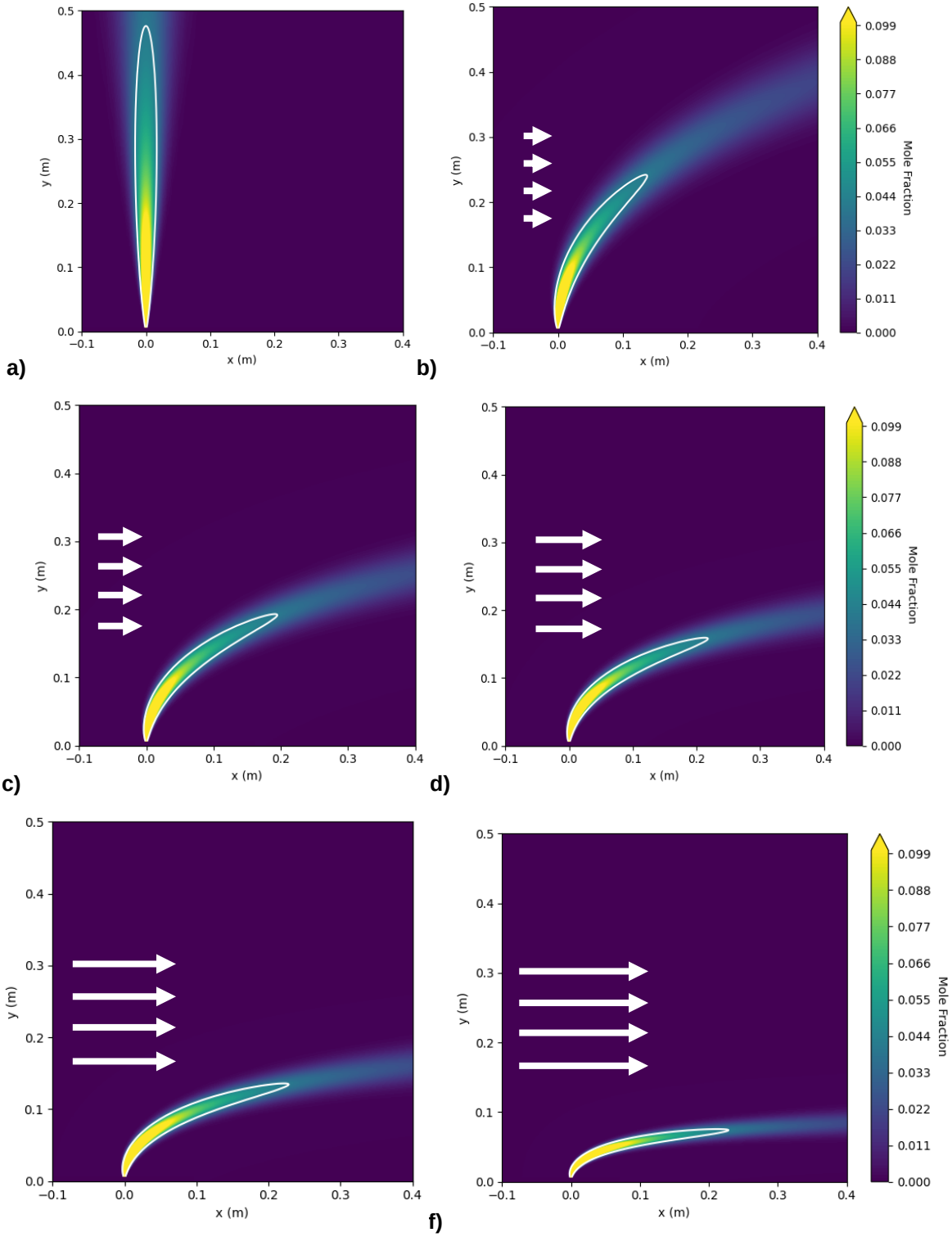


Figure 3-6. 4 mol% hydrogen concentration contours using HyRAM+ wind entrainment model, for hydrogen stored at 0.3 MPa (43 psi) and 25°C (77°F), released vertically through a 1 mm orifice, and subject to a) no wind, b) 10 m/s wind at a 0° angle, c) 20 m/s wind at a 0° angle, d) 30 m/s wind at a 0° angle, e) 40 m/s wind at a 0° angle, and f) 100 m/s wind at a 0° angle. Wind vectors shown are not to scale.

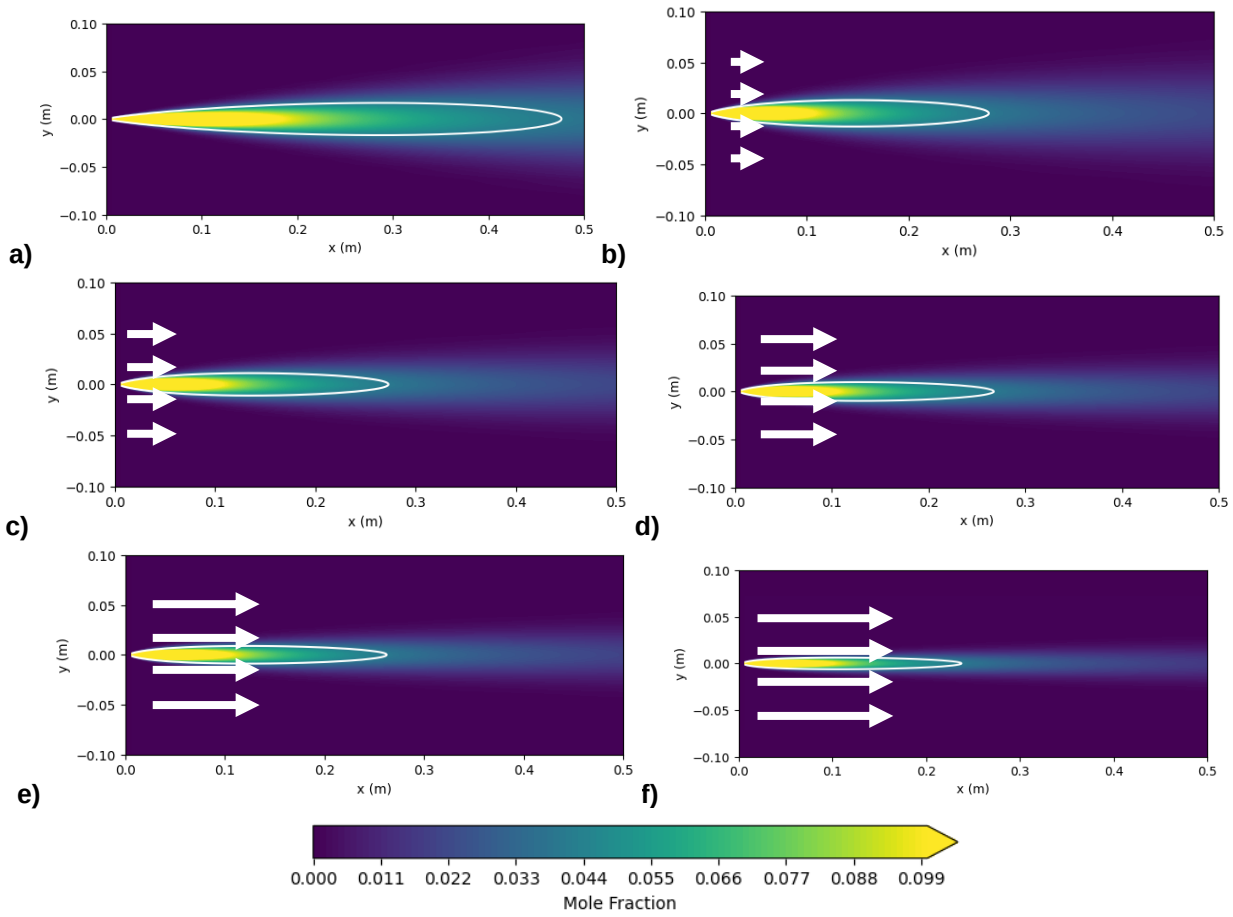


Figure 3-7. 4 mol% hydrogen concentration contours using HyRAM+ wind entrainment model, for hydrogen stored at 0.3 MPa (43 psi) and 25°C (77°F), released horizontally through a 1 mm orifice, and subject to a) no wind, b) 10 m/s wind at a 0° angle, c) 20 m/s wind at a 0° angle, d) 30 m/s wind at a 0° angle, e) 40 m/s wind at a 0° angle, and f) 100 m/s wind at a 0° angle. Wind vectors shown are not to scale.

Figure 3-6 and Figure 3-7 show the changing behavior of the plume when encountering different wind speeds for a vertically and horizontally discharged jet, respectively. Figure 3-6 shows the vertically discharged jet being subjected to a crossflow from horizontal wind and Figure 3-6 shows the horizontally discharged jet being subjected to a co-flow from a horizontal wind. In the crossflow case, the plume becomes more and more bent over in the direction of the wind as the wind speed increases. In the co-flow case, the plume becomes shorter and narrower as the wind speed increases. The decrease in plume length along the streamline is evident in both the crossflow and co-flow cases, with Figure 3-8 showing how the same wind speeds shorten the jet slightly more in co-flow than in crossflow conditions.

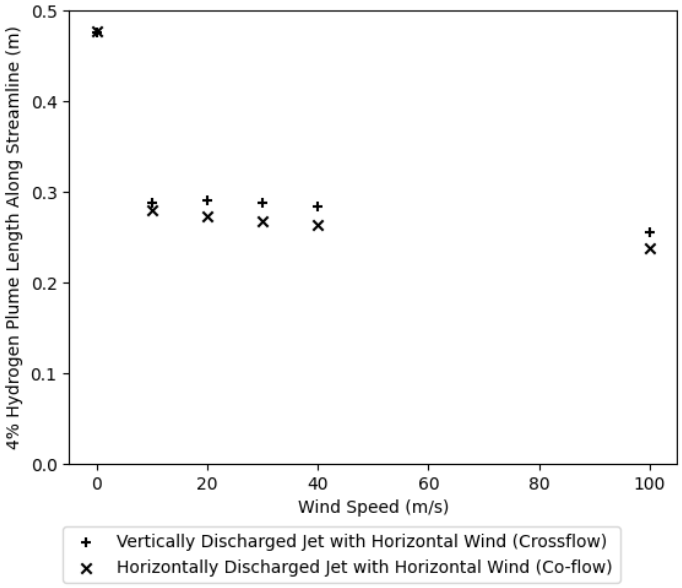


Figure 3-8. Plume streamline distance to 4 mol% hydrogen concentration for crossflow and co-flow conditions.

One major insight that can be gained from the HyRAM+ results is how the behavior of hydrogen compares to the behavior of comparably hazardous (flammable and combustible) fuels. The API document, Recommended Practice 521, (API RP 521) contains models for plume size in terms of both vertical height and downwind distance, for the crossflow experienced by vertical jets discharging into lateral ambient wind. These models are for "petroleum gases," which are not explicitly defined in the document, but examples of methane and hexane are given in the text. It is possible to model methane or hexane behavior using HyRAM+, but it is also possible that the coefficients for wind entrainment may be fuel specific, meaning that coefficients determined for one gas may not be accurate for another gas. One potential way to address this would be to validate the wind model not just for multiple conditions, but also multiple fuels. Because of the unknown composition of "petroleum gases" as well as the unknown applicability of the hydrogen wind entrainment model, simulations of methane or hexane in HyRAM+ were not run, but some results in API RP 521 were compared to simulations for hydrogen.

The plume streamline distance is defined by distance to the lower flammability limit concentration of the petroleum gases, which is stated as approximately 3 weight percent; the distances to this limit that are provided in this document are assumed to generally be applicable to petroleum gases even though the flammability limit varies across different species. The comparison of plume dimensions in the vertical and horizontal directions for the HyRAM+ hydrogen plumes and API RP 521 petroleum gas plumes is shown in Figure 3-9. Since the document does not include ambient or stored fuel conditions, the ambient temperature and pressure were assumed to be 25°C (77°F) and 101.325 kPa (14.7 psi) respectively and the stored temperature and pressure were assumed to be -243°C (-405°F) and 3000 kPa (435 psi) respectively.

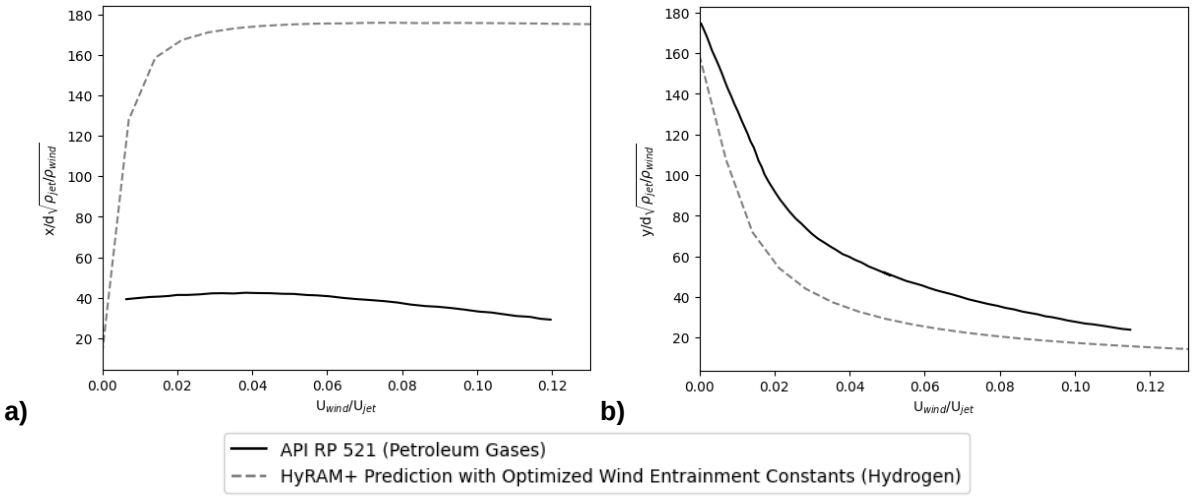


Figure 3-9. a) Downwind horizontal plume center distance and b) vertical plume center distance to the lower flammability limit for petroleum gases, provided in API RP 521, compared to hydrogen, calculated using HyRAM+.

The general trends of the two plots are similar – for the downwind horizontal plume center distance plot, there appears to be a large range of the tested wind-to-jet velocity ratios above a certain value where the horizontal distance that the plume travels downwind is fairly constant. The general decreasing vertical plume center distance with increasing wind-to-jet velocity ratios is also similar between API RP 521 petroleum gas predictions and the HyRAM+ hydrogen predictions. HyRAM+ seems to predict flammable distances that are longer in the downwind horizontal direction than API RP 521 predicts with petroleum gas plumes, but it predicts slightly shorter plumes in the vertical direction than the API RP 521 model calculates for petroleum gas plumes. If these trends are correct, they could have implications on hydrogen-specific equipment design or setback distances that would potentially be different from requirements for petroleum gases. However, data for both hydrogen and different hydrocarbon gases are needed to confirm that both models, trends, and insights are physically accurate. Furthermore, the API RP 521 model is only provided for a vertical jet in a perpendicular crosswind, so the model may not hold for other jet or wind angles. Parts of the API RP 521 model were also generated using observations from experiments done for a jet of air mixing in air, which means that there may be differences in the behavior of hydrocarbon plumes that were not accounted for [16].

As mentioned throughout this report, experimental data can be used to further refine the entrainment model and report trends and comparisons between fuels with more certainty. The experimental data taken by Grune et al., in a confined chamber where the wind speed and other ambient conditions could be controlled, is a logical starting point [15]. Testing a wider range of plume and wind directions and speeds would help validate or set boundary conditions for the wind entrainment model. Additionally, testing different orifice sizes and hydrogen backpressure and temperature could improve the understanding of any boundary conditions that may be needed for the hydrogen conditions for the wind entrainment model to be most accurate.

4. OTHER ENTRAINMENT MODELS

As discussed in Section 3.2, the models included in Gebhart et al. [7] include several models for a jet plume release into a flowing ambient from a single orifice point with consideration of momentum and buoyancy-driven ambient conditions. While not explicitly derived for a particular fluid or release into wind, the physical phenomena these models portray are still relevant to the assessment of entrainment here. The study in this section compares these entrainment models (henceforth referred to as the "Gebhart models") with the empirical wind entrainment model developed for this work (referred to as the "HyRAM+ model") to assess similarities and shortcomings of these models.

The Gebhart models are all based on the general form of entrainment for a flowing ambient devised by Hirst [17]. The terms for an unspecified ambient media are replaced by variables representing wind used elsewhere in this report for consistency:

$$E = 2\pi B[a_1 + (a_2/Fr_L)\sin\theta]\left[\left|v_{cl,plume} - v_{wind}\cos\theta\right| + a_3 v_{wind}\sin\theta\right]$$

Where B is the plume half-width, Fr_L is the local Froude number, θ is the relative angle between the jet plume release direction and the flowing ambient (i.e., $\theta = \theta_{jet} - \theta_{wind}$), $v_{cl,plume}$ is the velocity of the plume centerline, v_{wind} is the velocity of the wind, and a_1, a_2, and a_3 are empirically derived coefficients. The three variations of this form included in Table III from [7] are included in Table 4-1.

Table 4-1. Summary of entrainment models for flowing ambient conditions from Gebhart et al. [7]

Model	Entrainment equation
Hirst [17]	$E = 2\pi B[0.057 + (0.97/Fr_L)\sin\theta]\left[\left\|v_{cl,plume} - v_{wind}\cos\theta\right\| + 9v_{wind}\sin\theta\right]$
Ginsberg and Ades [18]	$E = 2\pi B[0.057 + (0.97/Fr_L)\sin\theta]\left[\left\|v_{cl,plume} - v_{wind}\cos\theta\right\| + \left\{25.81\left[Fr_{den}^{0.195}\left(\frac{v_{wind}}{v_0}\right)^{0.352}\right] - 10.83\right\}v_{wind}\sin\theta\right]$
Schatzmann [19]	$E = \frac{2\pi B[0.057 - (0.67/Fr_L)\sin\theta]\left[\left\|v_{cl,plume} - v_{wind}cos\theta\right\| + 2v_{wind}sin\theta\right]}{\left[1 + (5v_{wind}cos\theta)/\left\|v_{cl,plume} - v_{wind}\right\|\right]}$

All these models were integrated into the jet model in HyRAM+ and tested under the same hydrogen release conditions included above in Figure 3-2 alongside the selected HyRAM+ empirical wind entrainment coefficients discussed earlier ($c\parallel = 0.149$ and $c\perp = 0.00864$). The results from this comparison of jet plume contours across a range of wind directions and speeds are shown in Figure 4-1 through Figure 4-3. Overall, all the models show the same general contour in response to the various wind conditions, although the HyRAM+ model shows less entrainment compared to the Gebhart models. This is likely due to the inclusion of multiplication by the $[a_1 + (a_2/Fr_L)\sin\theta]$ term in the Gebhart models, which makes the entrainment constant proportional to the inverse local Froude number, which does not have an equivalent in the HyRAM+ model. The HyRAM+ model has the best agreement with the Schatzmann model, which was also derived entirely from best fit to empirical data, whereas the Hirst and Ginsberg models have a partial theoretical basis that simplifies to the quiescent ambient entrainment model included elsewhere in Hirst.

Testing the Gebhart models across a range of conditions in HyRAM+ also reveals limitations with these models. In particular, all the models show occasional sharp cutoffs in the far field, particularly

for conditions with strong winds and/or counter-flowing wind. This is due to the entrainment conditions creating stiff equations that the jet model in HyRAM+ cannot numerically solve without an inefficiently short spatial step. However, the trends and contours of the jet plumes are still clear in these cases given this behavior only occurring in the far field. Additionally, both the Hirst and Ginsberg models show unrealistic entrainment when the angle between the wind and hydrogen jet exceeds 90 degrees, with entrainment appearing to reduce to zero. This is a numerical artifact of the limited definitions of these models used in Gebhart et al.; these models were derived assuming the relative angle of the ambient flow along the axis of the release media, not with respect to the vector of release. As a result, the models mathematically do not account for relative angles greater than 90 degrees accurately. Notably, the comparisons of these two models in Gebhart et al. do not include any comparisons with greater than a 90-degree crossflow.

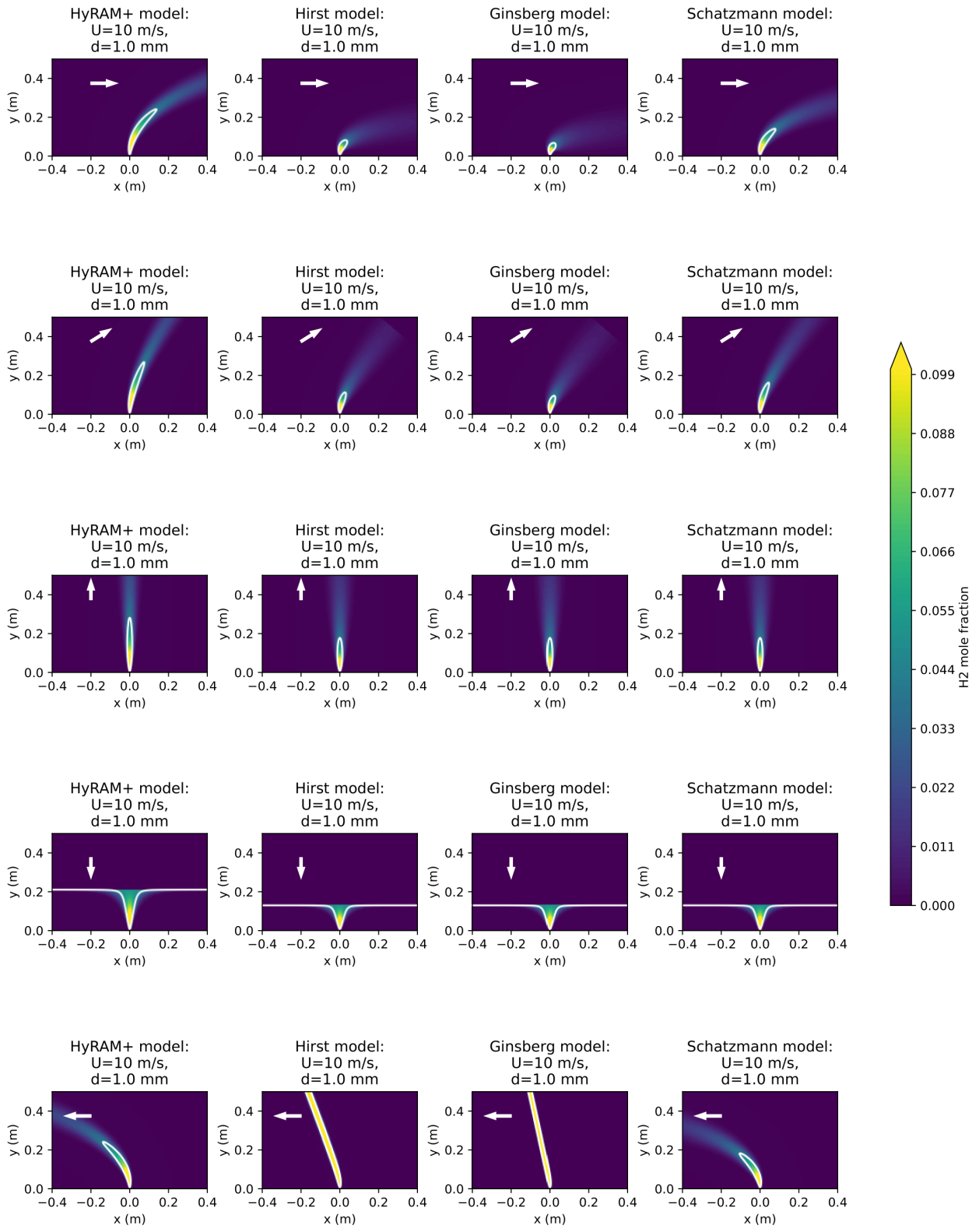


Figure 4-1. Entrainment model comparison, vertical release with varying wind directions (indicated by white arrow).

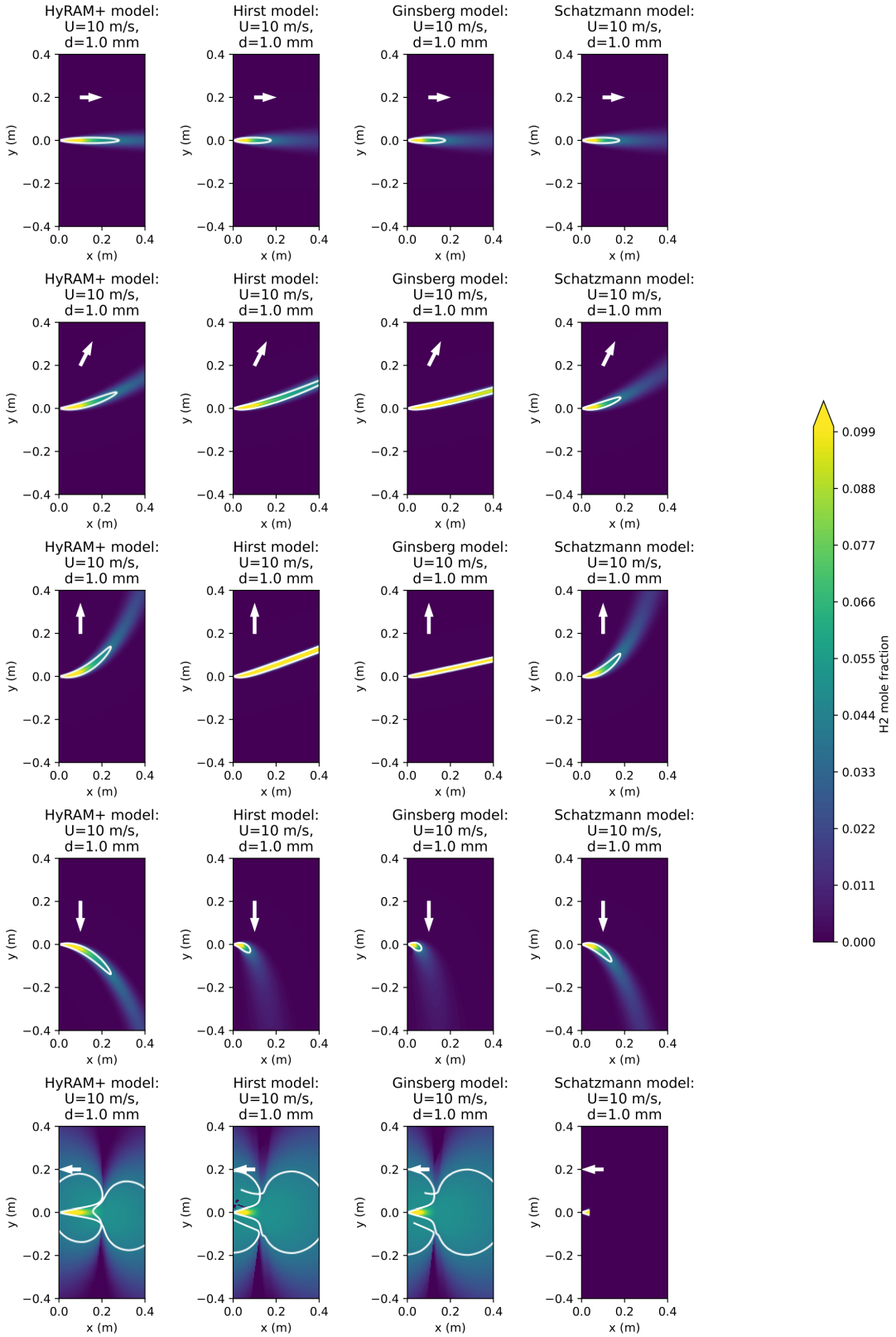


Figure 4-2. Entrainment model comparison, horizontal release with varying wind directions (indicated by white arrow).

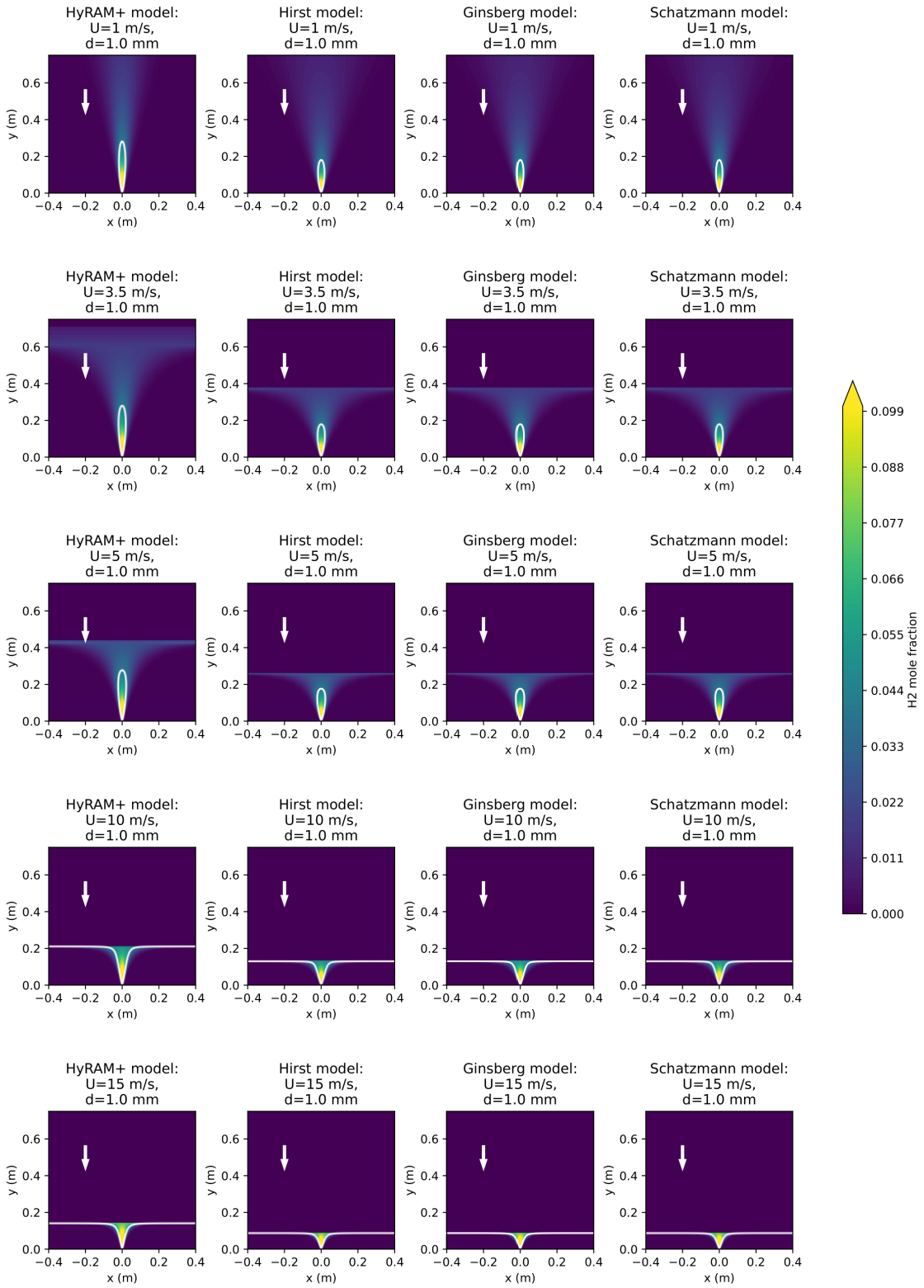


Figure 4-3. Entrainment model comparison, vertical release with counter-flowing wind of various speeds

Figure 4-4 compares the Gebhart models to the experimental data from Grune et al. [14] revealing that these models agree less than the HyRAM+ entrainment model, with the Schatzmann model agreeing somewhat better than the Hirst and Ginsberg. This again points to the need for more experimental data of jets in flowing ambient conditions to better tune the existing models; indeed, Gebhart et al. warns against using its models for flowing ambient conditions with a high level of confidence.

Overall, the entrainment models from Gebhart et al. show agreement in general behavior with the empirical entrainment model devised in this work, though all show greater entrainment than the HyRAM+ model, with less correlation with the Grune et al. experimental data. The Gebhart models also are also less stable than the HyRAM+ model, though these issues would not significantly affect the risk assessment of a hydrogen release. The more generic model currently used enables tuning to additional data and could be further modified if additional physics needs to be included. Overall, these results illustrate a need for more experimental data for these conditions to gain confidence in the models used to model flowing ambient conditions.

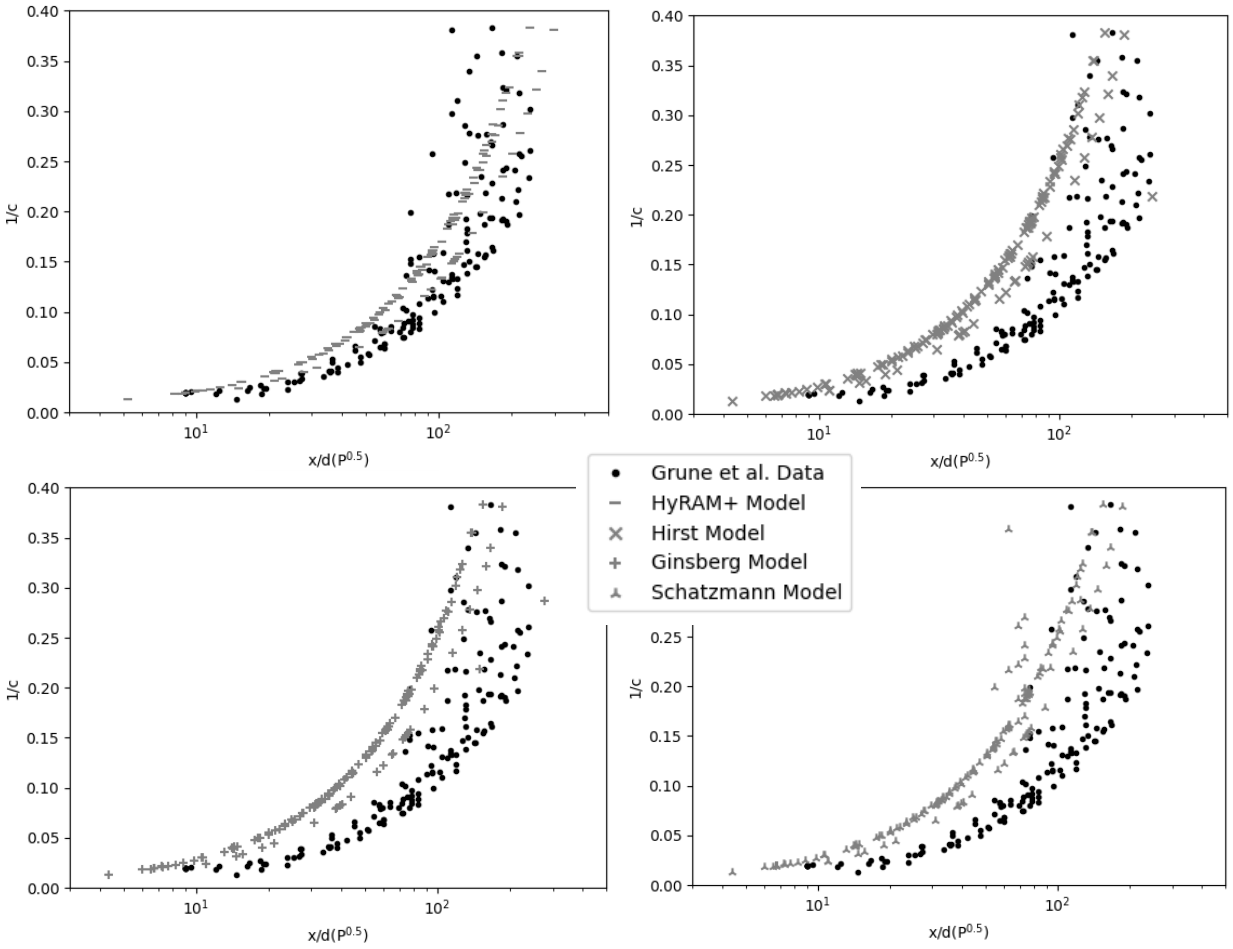


Figure 4-4. Comparison of entrainment models in Gebhart et al. [7] to experimental data from Grune et al. [15]

5. CONCLUSIONS

This report includes studies on two phenomena relevant for use of hydrogen fuel on locomotives: hydrogen releases through a vent stack and the effects of wind on hydrogen plume dispersion.

Modeling of the plume exiting the vent stack was performed by matching the vent stack effluent mass flow rate to the PRD effluent mass flow rate. Using this assumption, it was found that increasing the vent stack diameter led to decreased backpressures within the vent and increased lengths of the hydrogen plumes in the choked and unchoked flow regimes, but decreased lengths in the transition from choked to unchoked flow out the vent stack. If this trend does truly model the physical behavior of hydrogen plumes out of vent stacks, the increasing plume length with vent diameter could be due to decreased entrainment with lower exit velocities, meaning less turbulent mixing and dilution of hydrogen in air. Previous work has already been done to validate HyRAM+ calculations of plume characteristics such as length against experimental data, and the only difference in this study was simultaneous adjustment of pressure and orifice diameter due to the vent stack outlet. The trend found in the HyRAM+ results of increasing distance to the hydrogen flammable limit with decreasing Froude number is somewhat unexpected and was not consistently reflected in the literature; however, Froude number takes multiple physical parameters of the plume into account and may not be a sufficient indicator of whether the HyRAM+ results are physically accurate. Therefore, more validation work, either through identifying or performing vent stack release experiments, could be useful in determining whether the vent stack trends observed in this study reflect reality. Further validation with studies specific to vent stacks could also help confirm whether the potentially conservative assumption of constant mass flow rate through the vent is valid, and if other parameters such as vent stack length should be incorporated to improve the model.

Additionally, many of the existing published data on plume characteristics focus on the centerline profile (centerline concentration, velocity, density, etc.), but the results in this report show that the shape of the plume can be quite different even when the centerlines may be similar. The plumes from choked flow releases out of the vent stack tended to be narrower while the plumes from unchoked flow releases tended to be wider. Therefore, a search or experimental design for more holistic plume profiles besides the centerlines may be beneficial in explaining how contours are currently calculated, and if there should be any changes made. In general, fewer comparisons have been done for the predictive capabilities of HyRAM+ in unchoked flow regimes, and the work in this report helped highlight this area of ongoing study.

Second, HyRAM+ was used to model the behavior of a hydrogen plume when discharged into ambient wind. Model changes were made to the HyRAM+ code, including wind effects on the momentum governing equations and the entrainment model. The entrainment model was a generic model nonspecific to any fuel, but it was customized for hydrogen by adjusting two constants based on data from experiments in which hydrogen was released into a confined chamber with a controlled amount of wind. The fit resulted in a nonzero R^2 value, which indicated some relationship between the HyRAM+ model and the collected data and means there is promise in the HyRAM+ model used. The model showed that increased wind would bend the plume in the direction of the wind and shorten the plume, possibly due to increased entrainment, turbulent mixing, and hydrogen dilution introduced by the wind. Some visualizations of plumes in a flowing ambient seemed to have unexpected shapes, especially in the case of counter-flow. However, the trends and shapes of plumes in the other scenarios appeared to follow expected behaviors. This model was also compared to historical entrainment models for flowing ambient conditions. The contours of the results show

good agreement, though the model devised in this study shows reduced entrainment compared to the historical models.

While some literature was found for both topics, little existing data was found to validate the models tested in this report. There was insufficient quantitative data available for vent stack releases of hydrogen, and the data used to tune the wind entrainment model was limited in scope. Therefore, designing and conducting more controlled experiments directly relevant to locomotive applications could help validate and refine the vent stack and the wind models presented in this report.

REFERENCES

[1] B. Ehrhart, E. Hecht, and B. Schroeder, "Hydrogen Plus Other Alternative Fuels Risk Assessment Models (HyRAM+) Version 5.1 Technical Reference Manual," Sandia National Laboratories, SAND2023-14224, Dec. 2023.

[2] CGA G-5.5, "Standard for Hydrogen Vent Systems." Compressed Gas Association, Apr. 14, 2021.

[3] W. Houf and R. Schefer, "Analytical and experimental investigation of small-scale unintended releases of hydrogen," *International Journal of Hydrogen Energy*, vol. 33, no. 4, pp. 1435–1444, Feb. 2008, doi: 10.1016/j.ijhydene.2007.11.031.

[4] B. Ehrhart, E. Hecht, and J. Mohmand, "Validation and Comparison of HyRAM Physics Models," Sandia National Laboratories, SAND2021-5811, May 2021.

[5] S. H. Han, D. Chang, and J. S. Kim, "Release characteristics of highly pressurized hydrogen through a small hole," *International Journal of Hydrogen Energy*, vol. 38, no. 8, pp. 3503–3512, Mar. 2013, doi: 10.1016/j.ijhydene.2012.11.071.

[6] E. Hecht and N. Killingsworth, "Effect of Wind on Cryogenic Hydrogen Dispersion from Vent Stacks," presented at the International Conference on Hydrogen Safety, 2021.

[7] B. Gebhart, D. Hilder, and M. Kelleher, "The Diffusion of Turbulent Buoyant Jets," *Advances in Heat Transfer*, vol. 16, pp. 1–57, 1984, doi: 10.1016/S0065-2717(08)70203-X.

[8] X. Zhang and A. Ghoniem, "A Computational Model for the Rise and Dispersion of Wind-Blown, Buoyancy-Driven Plumes - I. Neutrally Stratified Atmosphere," *Atmospheric Environment*, vol. 27A, no. 15, pp. 2295–2311, Apr. 2023.

[9] T. Dürig, M. Gudmundsson, F. Dioguardi, and L. Steffensen Schmidt, "Quantifying the Effect of Wind on Volcanic Plumes: Implications for Plume Modeling," *Journal of Geophysical Research: Atmospheres*, vol. 128, no. 2, Jan. 2023, doi: 10.1029/2022JD037781.

[10] Z. Shu, W. Liang, F. Liu, G. Lei, X. Zheng, and H. Qian, "Diffusion characteristics of liquid hydrogen spills in a crossflow field: Prediction model and experiment," *Applied Energy*, vol. 232, Oct. 2022, doi: 10.1016/j.apenergy.2022.119617.

[11] API RP 521, "Guide for Pressure-Relieving and Depressuring Systems." American Petroleum Institute, Mar. 1997.

[12] *Areal Locations of Hazardous Atmospheres (ALOHA)*. Environmental Protection Agency. Accessed: Nov. 20, 2024. [Online]. Available: https://www.epa.gov/cameo/aloha-software

[13] R. Witcofski and J. Chirivella, "Experimental and analytical analyses of the mechanisms governing the dispersion of flammable clouds formed by liquid hydrogen spills," *International Journal of Hydrogen Energy*, vol. 9, no. 5, pp. 425–435, Aug. 2003, doi: 10.1016/0360-3199(84)90064-8.

[14] W. Buttner, J. Hall, S. Coldrick, P. Hooker, and T. Wischmeyer, "Hydrogen wide area monitoring of LH2 releases," *International Journal of Hydrogen Energy*, vol. 46, no. 23, pp. 12497–12510, Mar. 2021, doi: 10.1016/j.ijhydene.2020.08.266.

[15] J. Grune, K. Sempert, M. Kuznetsov, and T. Jordan, "Hydrogen Jet Structure in Presence of Forced Co-, Counter- and Cross-Flow Ventilation," International Association for Hydrogen Safety, 2021.

[16] J. F. Taylor, H. L. Grimmett, and E. W. Comings, "Isothermal Free Jets of Air Mixing with Air," *Chemical Engineering Progress*, vol. 47, no. 4, pp. 175–180, Apr. 1951.

[17] E. Hirst, "Buoyant jets discharged to quiescent stratified ambients," *Journal of Geophysical Research*, vol. 76, no. 30, pp. 7375–7384, 1971, doi: 10.1029/JC076i030p07375.

[18] T. Ginsberg and M. Ades, "Correlation for the entrainment function for near-field thermal plume analysis," Brookhaven National Laboratory, Upton, NY, Jun. 1975.

[19] M. Schatzmann, "An integral model of plume rise," *Atmospheric Environment*, vol. 13, no. 5, pp. 721–731, Jan. 1979.

DISTRIBUTION

Email—Internal

Name	Org.	Sandia Email Address
Ethan Hecht	8367	ehecht@sandia.gov
Kristin Hertz	8367	klhertz@sandia.gov
Brian Ehrhart	8854	bdehrha@sandia.gov
Chris LaFleur	8854	aclafle@sandia.gov
Melissa Louie	8854	mlouie@sandia.gov
Michael Devin	8921	mcdevin@sandia.gov
Technical Library	1911	sanddocs@sandia.gov

Email—External

Name	Company Email Address	Company Name
Laura Hill	laura.hill@ee.doe.gov	DOE HFTO
Chris Homison	chris.homison@wabtec.com	Wabtec
Christine Watson	christine.watson@ee.doe.gov	DOE HFTO

This page left blank

This page left blank



Sandia National Laboratories is a multimission laboratory managed and operated by National Technology & Engineering Solutions of Sandia LLC, a wholly owned subsidiary of Honeywell International Inc. for the U.S. Department of Energy's National Nuclear Security Administration under contract DE-NA0003525.